5-2022

Colloidal Monolayers for Concentration Light in Ultra-Thin Semiconductor Layers

Rachel Cherry
University of Arkansas, Fayetteville

Colloidal Monolayers for Concentrating Light in Ultra-Thin Semiconductor Layers

A thesis submitted in partial fulfillment
of the requirements for the degree of
Master of Science in Chemistry

by

Rachel Cherry
University of Arkansas-Fort Smith
Bachelor of Science in Chemistry, 2018

May 2022
University of Arkansas

This thesis is approved for recommendation to the Graduate Council.

_____
Robert Coridan, Ph.D.
Committee Chair

_____
Maggie He, Ph.D.
Committee Member

_____
Stefan Kilyanek, Ph.D.
Committee Member

_____
Julie Stenken, Ph.D.
Committee Member

Abstract:

Thin film semiconductors are used as photoconductive absorber layers for the development of broadband terahertz generation. Using a femtosecond laser pulse, the generation of a transient increase in the conductivity occurs by photoexciting conduction band electrons in the semiconductor. These thermalize through the emission of terahertz radiation. The route to terahertz generation is not particularly efficient as significant losses come from the absorption in the substrate that is beneath the photoconductive antenna layer. This work explores the application of hexagonally close-packed monolayers of chemically synthesized nanospheres as a potential light concentration method for ultra-thin films of GaAs and black phosphorus that are relevant to terahertz generation. A nanosphere layer can induce an advantageous scattering texture which can increase the effective path length of light transport through the thin film. The nanosphere layer can also induce a significant absorption increase through optical resonances that are caused by the periodic arrangement of hexagonally close-packed spheres. To aid in the study of these effects, we use finite element simulations of absorption in a model GaAs photoconductive layer since GaAs is the present standard photoconductive absorber layer. These simulations enable us to map the absorption resonances in the material as a function of the photoconductive absorber layer thickness and sphere diameter. We are also able to construct the equivalent materials to characterize the optical absorption increases in real, experimental systems. With the aid of these results, we will show that a simple light concentration strategy is able to generate a significant increase in light absorption. Through the increase in light absorption, an improvement of the light-to-terahertz power conversion efficiency is achieved.

Acknowledgements

I would like to thank my parents, Deborah and Terry Kramm, from whom I have learned the important of curiosity and to have a drive for following my passions. And I would like to thank my spouse, Lyle, for all his support through the challenges that graduate school offers. I would also like to thank my academic advisor and mentor, Dr. Robert Coridan, who has guided me through graduate school and many undergraduate professors, including Dr. Sayo Fakayode, for the encouragement and advice to aid in furthering my education. I would also like to thank my committee members: Dr. Robert Coridan, Dr. Maggie He, Dr. Stefan Kilyanek, and Dr. Julie Stenken for their invaluable guidance and advice. Lastly, I would like to thank the other students in the Coridan lab that provided me with priceless advice and encouragement.

Table of Contents

1. Introduction

Thin film semiconductors are used as photoconductive absorber layers for the development of broadband terahertz generation. Using a femtosecond laser pulse, the generation of a transient increase in the conductivity occurs by photoexciting conduction band electrons in the semiconductor. These thermalize through the emission of terahertz radiation. The route to terahertz generation is not particularly efficient as significant losses come from the absorption in the substrate that is beneath the photoconductive antenna layer.

Light concentration has many applications where a materials electronic properties dictate the need for the use of thin films, such as photovoltaics or two-dimensional materials (MoS_2, black phosphorus, etc.) where the electronic properties are dependent on the thickness of the material. These electronic properties are the set of parameters and representations that fully describe the state and behavior of the electrons in a material. However, for these materials, the absorption length is much longer than the thickness of the material.

Absorbing more photons in these thin film materials can be accomplished through the implementation of light concentration and scattering schemes. The implementation of a chemically synthesized self-assembled layer for light concentration in the ultrathin films aid in this challenge. The self-assembled layer is comprised of a hexagonally close-packed layer of chemically synthesized colloidal nanospheres. The colloidal layer is capable of scattering light into a more horizontal path. This enables more photons to be absorbed by the thin film semiconductor layer. The colloids can be deposited onto the substrate or thin film using the slow evaporation method. With this research, the goal is to determine whether adding a structured layer of nanospheres or the inverse structure onto a thin film semiconductor will increase the absorption of light through the increase in the optical path length.

Here, we describe our research into the use of a hexagonally close-packed monolayers of chemically synthesized nanospheres as a potential light concentration method for ultra-thin films that are relevant to terahertz generation. A nanosphere layer can induce an advantageous scattering texture which can increase the effective path length of light transport through the thin film. The nanosphere layer can also induce a significant absorption increase through optical resonances that are caused by the periodic arrangement of hexagonally close-packed spheres. Additional further development of the light scattering texture is also pursued through the development of a monolithic structure that builds off a monolayer of spheres. To aid in the study of these effects, we use finite element simulations of absorption in a model GaAs photoconductive layer since GaAs is the current standard photoconductive absorber layer. These simulations enable us to map the absorption resonances in the material as a function of the photoconductive absorber layer thickness and sphere diameter. We are also able to fabricate the equivalent materials to characterize the optical absorption increases in real, experimental systems. With the aid of these results, we will show that a simple light concentration strategy is able to generate a significant increase in light absorption. Through the increase in light absorption, an improvement of the light-to-terahertz power conversion efficiency is achieved.

The development of this light scattering texture requires exploration of a multitude of variables. The structure of the light scattering texture needs to be reviewed to determine whether the sphere or inverse sphere layer aids more of an increase in absorption. If there is an increase in absorption, how large of an increase does the specific scattering layer give and does diameter of the sphere change the amount of absorption? If there is not an increase in absorption, is there a resonance in which an increase in reflection occurs and at what wavelength does this occur due to opalescence? Exploring the potential of different materials being used with different refractive

indices, is there a different in absorption into the semiconductor layer and can these structures be designed to further optimize the increase in the absorption. Aid in exploring these questions is done via finite-difference time-domain simulations. These simulations enable us to map the absorption resonances in the material as a function of the photoconductive absorber layer thickness and sphere diameter. We are also able to construct the equivalent materials to characterize the optical absorption increases in real, experimental systems.

The motivating application for this work is the development of a light stimulated terahertz-emission from a photoconductive antenna device. These devices can be used in place of x-ray sources for medical imaging application. Current medical imaging technologies, such as x-rays or computed technology (CT) scans, use x-rays to see the sizes, shapes, and position of portions of the body. X-rays can be found on the electromagnetic spectrum at a higher frequency than that of visible and ultraviolet light. Due to the high energy of the x-ray photons, ionization occurs on molecules in the body. When an x-ray photon encounters an electron, the electron is ejected from its quantum state which can disrupt molecular bonds and ionize atoms. Exposure to large amounts of x-rays over a period of time can cause cancer to form.[1]

The remainder of this work is organized in chapters as follows. Chapter 1 covers the important background information for the general understanding of the electromagnetic spectrum, terahertz, and its importance, how a terahertz device works, overview of semiconductors, and what this work accomplishes. Chapter 2 is a literature review of terahertz devices, plasmonics, photonics, and different methods of colloidal deposition. Chapter 3 focuses on the development and work of a black TiO_2 thin film, and the absorption increase obtained by monolayers of spheres. Chapter 4 is the finite-difference time-domain simulations for

determination of specific materials and structures to use for the development of the monolith structure and Chapter 5 is the conclusion for summarization of the work.

References

(1) Berger, M.; Yang, Q.; Maier, A. X-ray Imaging. In *Medical Imaging Systems: An Introductory Guide*, Maier, A., Steidl, S., Christlein, V., Hornegger, J. Eds.; Springer International Publishing, 2018; pp 119-145.

2. From the electromagnetic spectrum to semiconductors of a terahertz device

2.1 The electromagnetic spectrum and terahertz

The electromagnetic spectrum is comprised of the electromagnetic radiation according to either its frequency or wavelength. While all electromagnetic waves on the spectrum travel at the speed of light (299,792,458 m/s) in a vacuum, they do this at a wide range of wavelengths, frequencies, and photon energies. Figure 2.1 shows the various subranges of the electromagnetic spectrum, such as visible light or microwaves. Each of the subranges given will have different types of interactions. The x- and gamma-rays excite electrons with such high levels of energy that the electrons are ejected out of their quantum states which ionizes the molecules in which it encounters. The UV and visible light regions excited electrons to different electronic states. The infrared region can show the different molecular vibrations that various molecules have. The molecular vibrations correspond to the different movements (stretching and bending) of the bonds between atoms. The terahertz region is low energy vibrational modes associated with the intermolecular interactions. Microwaves interact with matter, except for metallic conductors, by causing molecules to rotate and produce heat as the molecules rotate. With metallic conductors, microwaves are strongly absorbed as well as lower frequencies and will cause the electrical currents that heat the material. Radio waves have some relevance with NMR as well. NMR spectroscopy uses radio frequency waves to promote transitions between nuclear energy levels.[1]

Terahertz (THz) is a region in the electromagnetic spectrum that lies between microwave (1mm) and far infrared bands (100μm) with this region being shown in Figure 2.1.[2,3] Far infrared band is the region of infrared light in which the wavelengths are 10^{-4}m. One of the earliest commercial uses of THz imaging and spectroscopy is the nondestructive screening of

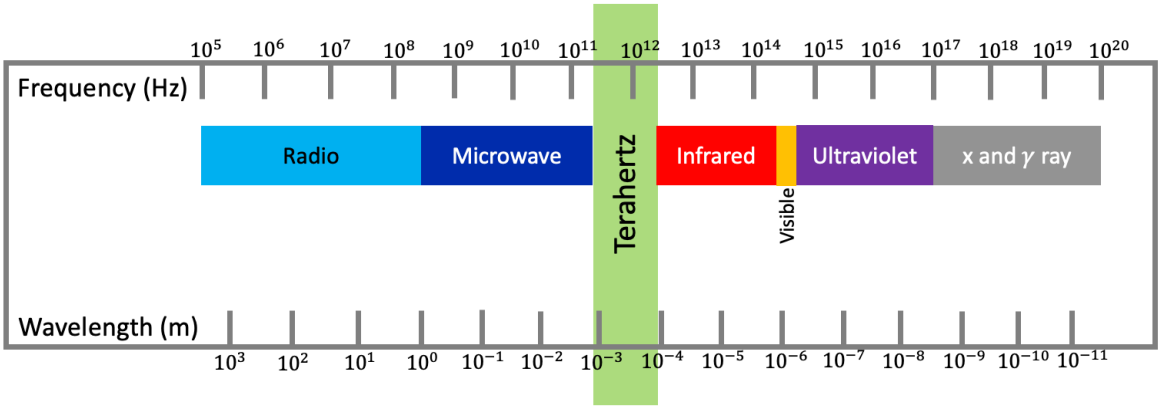

Figure 2.1 The electromagnetic spectrum.

pharmaceuticals where the changes in solid state crystal form and spectral fingerprinting of different chemical compounds were demonstrated. Spectral fingerprinting also has the potential applications in security as well. The largest application of interest is the potential for a nonionizing medical imaging method which is an alternative to an x-ray without the cancer-causing radiation. While x-rays are capable of detecting a multitude of issues, most of them are related to the skeletal structure with dislocations, infections, breaks/fractures, and arthritis.[2] Although both can be used for imaging, there is a difference in the energies of the photons for each source. THz photons containing an energy range of 1-100meV while an x-ray photon typically has an energy range of 10-10,000eV. The lower photon energy of THz typically does not damage living tissue and DNA like x-rays could while still being able to penetrate through the skin. THz imaging would be able to discern the difference between healthy and cancerous tissue due to the increase in blood and water in cancerous tissue since water absorbs THz.[4]

2.2: Terahertz Devices

While these applications show promise, harnessing the capabilities of THz generation in an effective manner comes with its own challenges. Development of THz generation has been a difficult process, especially when trying to obtain a broadband THz emission which can span a range of frequencies.[5] THz lies between microwaves and infrared regions on the electromagnetic spectrum. Approaching this regime from either of these regions comes with its own unique challenges. Increasing the operating frequency of microwave devices is limited by carrier mobility of the oscillating semiconductor. Reducing the energy of the emitted photons in the infrared region generated by electron transitions within a semiconductor is inhibited due to THz photons having less energy than the thermal energy at room temperature.[2]

The generation/detection of THz is achieved using photoconductive antennas in which electrons are optically pumped to through the excitation of electrons. As shown in Figure 2.2, the photoconductive antenna is pulsed with an incident light, typically an ultrafast laser pulse, at the gap between the electrodes. The THz emitter has a voltage bias through a direct current voltage between the electrodes. The incident light excites electrons that are accelerated along the direct current bias. The electrons then lose their energy which powers the antenna that emits the THz pulse.[2]

The generation of the pulsed THz radiation begins with a femtosecond optical pulse on a photoconductive antenna. The device consists of an anode and cathode that are patterned on a photoconductive substrate. The optical laser pulse is positioned on the antenna gap and propagates into the photoconductor. This begins the generation of photocarriers within the photoconductor upon absorption. Subsequently, the generated photocarriers will lose energy via scattering off atoms and defects in the material and the energy loss will form the THz emission.[2] The photoconductive substrate is a material, such as a semiconductor, that becomes more electrically conductive due to the absorption of electromagnetic radiation. Typically, this is ultraviolet, visible, or infrared light.[6]

2.3: Semiconductors

A semiconductor is a material that has the properties from both conductors and insulators. The differences of the three is the band gap between the valence and conduction bands as shown in Figure 2.3. The valence band consists of mostly filled electronic states and the conduction band consists of mostly empty valence electronics states which are analogous to the HOMO and LUMO levels in molecules. The energy difference between the valence and conduction band

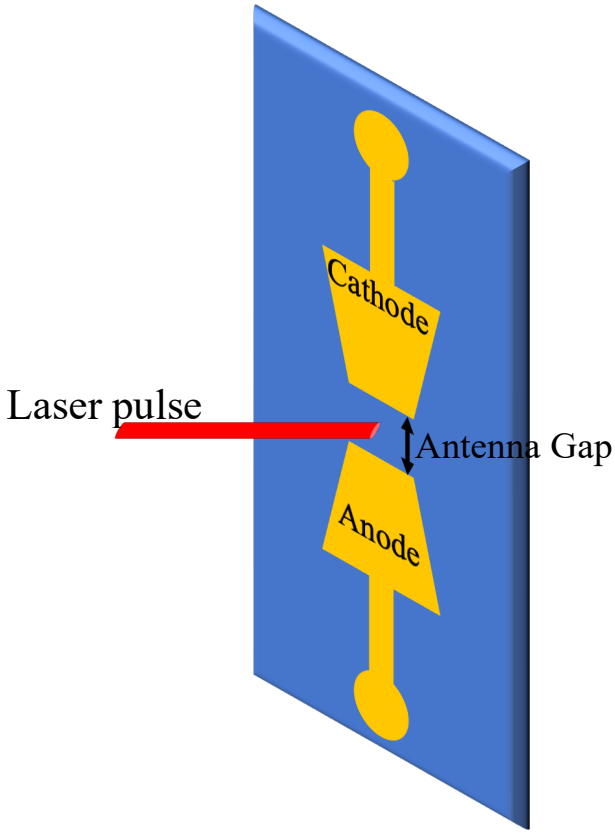

Figure 2.2 Example of a terahertz photoconductive antenna.

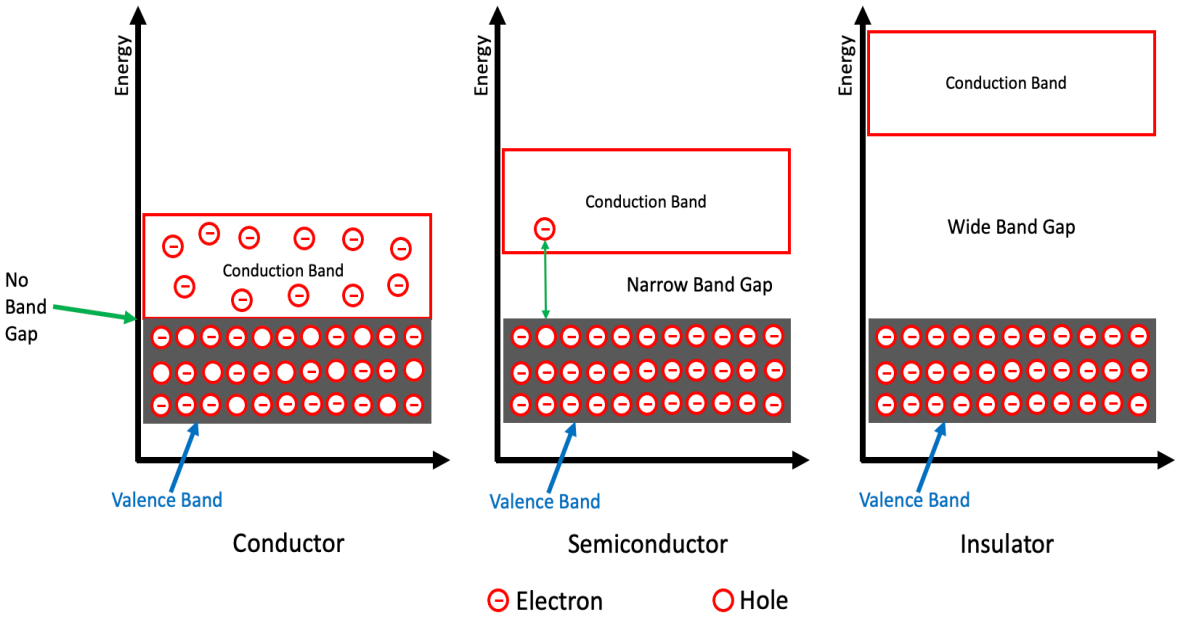

Figure 2.3 Schematic of a conductor (left), semiconductor (middle), and insulator (right).

edges are called the band gap. The band gap sets the physical limit on the minimum energy a photon must have to excite the electrons is the band gap. The larger the gap is, the more difficult it becomes to excite the electrons from the valence band into the conduction band. In a conductor, electrons are easily excited into the conduction band via thermal excitation that occurs at room temperature. An example of a conductor is copper due to its lack of a band gap. Semiconductors require a specific amount of energy to excite the electrons into the conduction state. A few electrons can be excited into the conduction band at room temperature, unlike insulators. An example of a semiconductor is silicon which has a band gap of 1.12eV. To excite an electron into the conduction band, the electron must absorb a minimum of 1.12eV. The average thermal energy of an electron at room temperature is 0.0259eV. Insulators have such a large band gap that it is very difficult to excite electrons enough for them to move to the conduction band. An example of an insulator is diamond with a band gap of 5.47eV. Due to the large band gap, electrons cannot readily move through it.[7]

Development of semiconductors into thinner films using a two-dimensional material (black phosphorus or MoS_2, for example) has been of recent interest and is advantageous for THz antennas. The two-dimensional materials have band gaps that change depending upon the number of layers there are. These two-dimensional materials are also capable of exhibiting high optical absorption and responsivity and high carrier mobility which supersede previously used semiconductor materials like GaAs.[8] Using a thinner film will also keep the THz emission from being absorbed by the photoconductive layer. Absorption of the pulse by the semiconductor layer causes a weaker pulse to occur. While this aids in maintaining the THz pulse, the thin film semiconductor comes at a cost. Much of the incident light is either reflected out of the layer or passes through the thin film before it is absorbed in comparison to their thick substrate-based

counterparts. One way to determine the amount of light that is absorbed is through the absorption coefficient which depends on the material and the wavelength of light being absorbed. The absorption coefficient is defined as the intensity attenuation of the light passing through a material and can be understood as the sum of the absorption cross-section per unit volume of a material for an optical process. The higher the absorption coefficient, the shorter length the light must penetrate the semiconductor before it is absorbed. With a material that has a low absorption coefficient, light is only poorly absorbed. If the material is thin enough, this can cause the material to appear transparent to that wavelength.[9]

Semiconductors have two different types of band gaps: direct and indirect. A direct band gap has the same value of momentum at the bottom of the conduction band and the top of the valence band for an electron and hole. This allows for the emission of a photon to occur causing the electron to recombine with the hole in the valence band. An example of a direct band gap is GaAs. In the indirect band gap, the momentum of the valence and conductance bands are offset. The maximum energy of the valence band occurs at a different momentum to the minimum of the conduction band energy. The electron is not only required to interact with the photon but must also interact with a lattice vibration (phonon) to either gain or lose enough momentum to recombine with the hole in the valence band. An example of an indirect band gap is germanium.[10]

In this work, black phosphorus is the material that will be used in place of the GaAs used in previous works. To achieve the appropriate band gap for black phosphorus, the film thickness must be thin (less than 100nm in thickness).[8] To improve the absorption of photons into the thin film, the use of light trapping scheme can aid in scattering and concentrating the incident light just above the thin film and therefore lengthening the optical path length of the light. By

redirecting the light into non-normal directions, this can give the film an appearance of being thick and allow for the absorption of photons to be increased.[11] The light trapping scheme chosen is the use of an ordered sphere layer comprised of a hexagonally close-packed layer of nanospheres (colloids).

References

(1) Andrews, D. L. Electromagnetic radiation. **2010**.

(2) Burford, N. M.; El-Shenawee, M. O. Review of terahertz photoconductive antenna technology. *Optical Engineering* **2017**, *56* (1), 010901.

(3) Federici, J. F.; Gary, D.; Barat, R.; Michalopoulou, Z.-H. Chapter 11 - Detection of Explosives by Terahertz Imaging. In *Counterterrorist Detection Techniques of Explosives*, Yinon, J. Ed.; Elsevier Science B.V., 2007; pp 323-366.

(4) Kawano, Y. 13 - Terahertz nano-devices and nano-systems. In *Handbook of Terahertz Technology for Imaging, Sensing and Communications*, Saeedkia, D. Ed.; Woodhead Publishing, 2013; pp 403-422.

(5) Chen, M.; Wu, Y.; Liu, Y.; Lee, K.; Qiu, X.; He, P.; Yu, J.; Yang, H. Current-Enhanced Broadband THz Emission from Spintronic Devices. *Advanced Optical Materials* **2018**, *7*, 1801608. DOI: 10.1002/adom.201801608.

(6) DeWerd, L. A.; Moran, P. R. Solid-state electrophotography with Al2O3. *Medical Physics* **1978**, *5* (1), 23-26, https://doi.org/10.1118/1.594505. DOI: https://doi.org/10.1118/1.594505 (acccessed 2022/03/06).

(7) Kita, T.; Harada, Y.; Asahi, S. Fundamentals of Semiconductors. In *Energy Conversion Efficiency of Solar Cells*, Springer, 2019; pp 157-202.

(8) Batista, J. S.; Churchill, H. O. H.; El-Shenawee, M. Black phosphorus photoconductive terahertz antenna: 3D modeling and experimental reference comparison. *Journal of the Optical Society of America B* **2021**, *38* (4), 1367-1379. DOI: 10.1364/JOSAB.419996.

(9) Gong, J.; Krishnan, S. Chapter 2 - Mathematical Modeling of Dye-Sensitized Solar Cells. In *Dye-Sensitized Solar Cells*, Soroush, M., Lau, K. K. S. Eds.; Academic Press, 2019; pp 51-81.

(10) Seo, D.-K.; Hoffmann, R. Direct and indirect band gap types in one-dimensional conjugated or stacked organic materials. *Theoretical Chemistry Accounts* **1999**, *102* (1), 23-32. DOI: 10.1007/s002140050469.

(11) Burford, N. M.; Evans, M. J.; El-Shenawee, M. O. Plasmonic Nanodisk Thin-Film Terahertz Photoconductive Antenna. *IEEE Transactions on Terahertz Science and Technology* **2018**, *8* (2), 237-247. DOI: 10.1109/TTHZ.2017.2782484.

Chapter 3: Literature Review of THz devices, plasmonics, photonics, and methods for colloidal deposition

This chapter focuses on the overview of a photoconductive antenna approach to THz, photonics, plasmonics, and deposition methods for colloids onto a surface. The first section reviews what the photoconductive antenna approach to THz is, how it works, and what has been done in previous works. These previous works will discuss all aspects of the development of the THz antennas while pinpointing areas for improvement. Plasmonics and photonics are two ways in which an increase in absorption of light into the semiconductor layer of the THz antenna. Plasmonics is a previously used method for THz while photonics has not been as heavily studied. In the photonics section, a comparison of different light trapping methods is done to aid in the absorption into a thin film semiconductor for the best fit. The final section will review different methods of colloidal deposition.

3.1: Photoconductive antenna approach to THz

Terahertz (THz) is the region in the electromagnetic spectrum that lies between the microwave band and the far infrared band. The THz portion of the electromagnetic spectrum is generally defined as the band of wavelengths between 1mm and 100μm, which correspond to frequencies of 1×10^{11} and 1×10^{12} Hz. THz gives the option for a nondestructive and nonionizing version of x-rays making it a better alternative for various applications such as security, THz imaging and spectroscopy, and medical imaging.[1] The difference in photon energy of one THz photon and one x-ray photon is significantly different as x-rays have much higher energy photons. One THz photon contains an energy range of 1-100meV while one x-ray photon typically has an energy range of 10-10,000eV. The lower photon energy of THz typically does

not damage living tissue and DNA like x-rays could while still being able to penetrate through the skin. While x-rays can pierce further into the skin, THz typically only have a millimeter penetration thickness into skin due to the strong attenuation by water and its sensitivity to water content. Due to the increase blood supply and water in the cancerous tissue, THz would be able to differentiate cancerous tissue from normal, healthy tissue.[2,3]

Emission and detection of pulsed broadband THz radiation from an optically pumped photoconductive antenna was first accomplished in the 1980s. A photoconductive antenna could be thought of as an electrical switch that exploits the increase in electrical conductivity of semiconductors when they have been exposed to an incident light. The photoconductivity is a result from the increase in the number of free carriers (electrons and holes) that are generated by the absorption of photons. The switch-on time is a function of the duration of the laser pulse while the switch-off depends on the carrier lifetime of the semiconductor.[4]

Some of the materials used for the semiconductor layer include bulk gallium arsenide (GaAs) and bulk indium gallium arsenide (InGaAs). Of the two, GaAs has been the preferred material for PCAs as it has a room temperature band gap of 1.424eV with an absorption length of approximately 870nm. This specific band gap allows for the use of a laser at a wavelength of 800nm. A laser with a wavelength of 1.55μm has also been tested with low temperature grown GaAs, however the results show a significant reduction in the performance in comparison to the 800nm laser.[1,5] Low temperature grown GaAs that is grown in temperatures between 200 and 250°C have two main benefits. Those are excess As^{3+} within the crystal structure which manifest as point defects and a high level of crystallinity. The point defects can act as recombination and trapping centers. These contribute to the reduction of carrier lifetimes through the act of recombination sites and higher carrier mobility respectively.[6]

InGaAs has also been studied as a potential photoconductive absorber for the THz antenna design.[1] Unlike GaAs, InGaAs has a benefit of potentially achieving a 0.8eV room temperature band gap.[5] Lower band gaps allow higher wavelengths for optical excitation meaning the use of a 1.55μm wavelength pulsed laser system can be done. However, to combat the low amount of effective recombination sites, iron doping was introduced to increase the number of recombination sites. While both materials have their own advantages, having a bulk layer means that some of the THz emission will be absorbed by the semiconductor layer in turn causing the emission to be weaker.

The use of two-dimensional materials for the semiconductor in THz as a light absorber has become a new interest in the field. These materials exhibit tunable optoelectronic properties that cause them to stand out as potential candidates. These two-dimensional materials exhibit high optical absorption and responsivity, as well as sub-picosecond carrier lifetimes and a high carrier mobility. Of these materials, black phosphorus has begun to receive substantial research interest for use in THz devices. Black phosphorus has a crystalline structure that consists of two axes with armchair and zigzag configurations. Black phosphorus also has a thickness dependent direct band gap. This band gap ranges from 2eV for a single layer to 0.3eV for a bulk configuration of black phosphorus.[7]

Overall, the need for thinner film materials is of great importance. The need for thinner films will keep the THz emission from being absorbed by the semiconductor layer. While this is not the only reason for the need of thin films, it is still substantial. Another reason that using thinner films is important is the implementation of two-dimensional materials, such as MoS_2 or black phosphorus. These two-dimensional materials exhibit high optical absorption and responsivity, sub-picosecond carrier lifetimes, and high carrier mobility. While these are

important strengths, these materials also typically have a thickness dependent band gap that changes with the thickness of the material which also gives rise to the importance of using thinner materials as the thinner the two-dimensional material is, the better the band gap becomes as it is more of a direct bandgap. For example, the black phosphorus band gap has a range of 2eV for the single layer to 0.3eV for the bulk configuration.[7]

3.2: Plasmonics

Plasmonics is a way to generate, detect and manipulate signals at high optical frequencies along a metal dielectric interface at nanometer scale. This method works to miniaturize current optical devices in applications such as sensing, microscopy, and optical communications.[8] Plasmonics typically utilize surface plasmon polaritons. Polaritons are hybrid particles that consist of a photon that is strongly coupled to an electric dipole. The surface plasmon polaritons have a constant phase relationship of electron oscillations that travel together along either a metal-dielectric or metal-air interface. Surface plasmon polariton describes that the wave involves both the charge motion in the surface plasmon (metal) and the electromagnetic waves in the air or dielectric. These are strongly confined to the supporting interface which gives rise to strong light-matter interactions.[9]

One specific example using this method that directly applies to increasing the THz pulse was completed by El-Shenawee's group. Their work combined plasmonic nanostructures with a thin film photoconductive layer in the development of novel PCAs. The fabrication process of the device requires a multistep process that is completed as follows and shown stepwise in Figure 3.1 from reference [10] by Burford et al. First, the creation of a low temperature grown GaAs layer is done through molecular beam epitaxy.[10] Molecular beam epitaxy is a process in

which a thin single crystal layer is deposited onto a single crystal substrate via atomic or molecular beams that are generated in a Knudsen cell that is contained in an ultrahigh vacuum chamber.[11] An Si-GaAs substrate is coated with a 300nm thick layer of $Al_{0.85}Ga_{0.15}As$ followed by a 10nm coating of AlAs and 120nm of low temperature grown GaAs. The low temperature grown GaAs is grown at a temperature of 250°C with a post growth annealing at 525°C for 10 minutes. After the annealing process is complete, the antenna pattern was deposited on the surface of the low temperature grown GaAs. The antenna electrode pattern was deposited using a standard image reversal photolithography process followed by 15/120-nm Ti/Au metal evaporation. The low temperature grown GaAs sample was then flip-mounted onto an HRFZ-Si substrate with the antenna electrode side down facing the HRFZ-Si substrate to be precured for 15 minutes at 100°C.

Removal of the low temperature grown GaAs layer from the host substrate is done through a combination of mechanical lapping and selective chemical etching. A second photolithography and etching process was utilized to electrically connect to the device antenna electrodes. The last step of the fabrication process is the deposition of the patterned nanodisk structure. The nanodisk structure was completed using electron beam lithography patterning and 5/40-nm Ti/Au metal deposition of the nanodisk array to the surface of the low temperature grown GaAs. The final device structure is shown in Figure 3.1(f) from the El-Shenawee group, reference [10].[10]

The plasmonic nanodisk array was computationally optimized prior to development for the purpose of localizing the incident optical field in the low temperature grown GaAs thin film layer. The computations done to optimize the structure of the nanodisk array using the

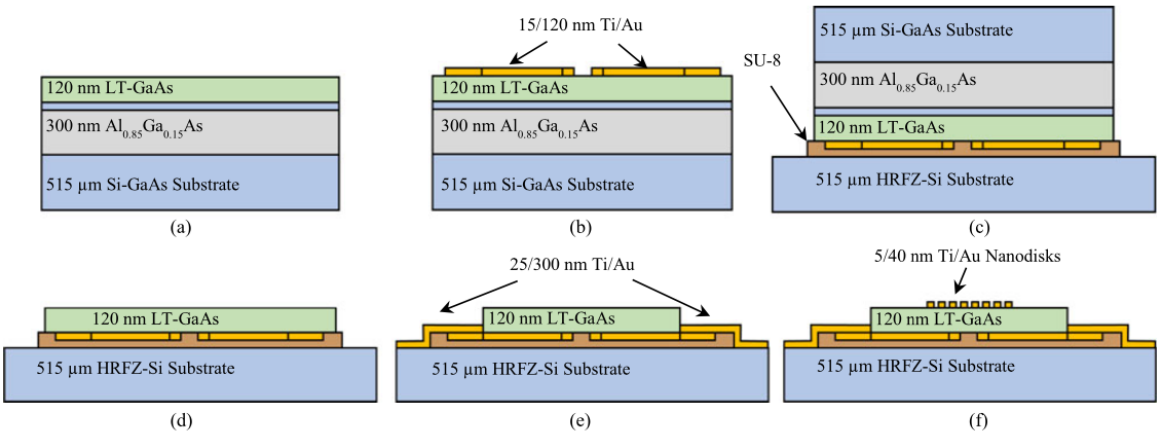

Figure 3.1 Step by step schematic representation of the development process of a terahertz device with a plasmonic nanodisk array. Final structure of the device is shown in part (f). (Reprinted with permission from reference 10. Copyright © 2018 IEEE.)

commercial finite-element method package of COMSOL Multiphysics. The nanodisk array was optimized for an 800nm wavelength optical excitation in which the main goal was to maximize the average electrical field inside the low temperature grown GaAs layer. An increase in THz pulses emitted from the plasmonic thin film PCA device was obtained when compared to conventional PCAs and was able to demonstrate a usable bandwidth nearing 5THz. While their findings showed improvement, there is still room for more improvement throughout.[10]

While the fabrication process is a complicated multistep process, there are some aspects of the design that can cause issues. One of the main drawbacks to the antenna electrodes and nanodisk array being constructed of gold is that gold can be reflective. Another problem is that gold will also absorb some of the energy from the laser pulse as well. This causes lower amounts of light to be absorbed and in turn causing a lower terahertz emission.

3.3: Photonics

Photonics is the science of light where the shaping of dielectric structures with a refractive index contrast aids in controlling the transport of light at a nanoscale level. Photonics typically deals with light from the infrared and visible light regions of the electromagnetic radiation spectrum. Photonics for this application, references the use of light to excite electrons in a semiconductor through periodic dielectric structures to increase photon absorption. One way to explain how these structures aid in the absorption of photons is through Snell's law. Snell's law predicts how the incident light can change direction as it passes from one medium (such as air or a metal) into another, or as it's reflected from the interface between two media. When incident light hits a flat surface of a new material at an angle, the light will bend away from the incident light[12] as shown in Figure 3.2.[13] However, when the incident light comes in

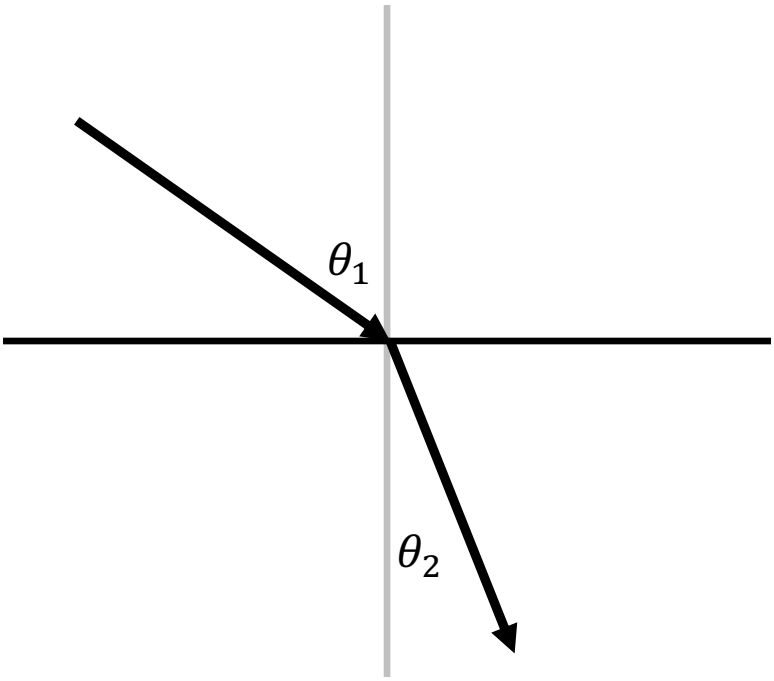

Figure 3.2 Schematic representation of Snell's law showing how light moves through various media differently.

perpendicular to the surface, then the light will continue straight through. Snell's law relates the angles of incidence, transmission, and reflection with the refractive indices at the interface. The refractive index is a measure of the velocity of light through a specific material. When determining the speed of light (299,792,458m/s) as it goes through a material, it is determined by multiplying the index of refraction of the material by the speed of light. Some examples of materials used to develop the device include polystyrene, quartz, and silicon. Polystyrene has an index of refraction of 1.55, quartz is 1.4, and silicon is 3.88. Air is another important index of refraction to know which is 1.00. When light enters a material with higher refractive index, the angle of refraction will be smaller than the angle of incidence and the light will be refracted towards the normal of the surface. The higher the refractive index, the closer to the normal direction the light will travel.[12]

Snell's law can aid in ray tracing to compute angles of the incidence light or refraction. Snell's law is one of the primary equations used in ray tracing as it governs the change in the direction of the ray at a dielectric interface between two materials. Ray tracing is a method for calculating the path of light through a system in which there are different regions that have varying refractive index (n) and absorption characteristics (such as the extinction coefficient, k). The change of n and k values at an interface control the vector components of the transmitted and reflected components of the ray at the interface. One way to calculate this is through Maxwell's equations which dictate the propagation of electromagnetic radiation, though we use other methods as described below. Understanding the pattern in which light moves through a material like silicon or polystyrene will aid in the development of a light trapping scheme that can concentrate the incident light near the surface of the semiconductor.[14] Light scattering is the process in which small particles (colloids, etc.) scatter light which in turn can cause an optical

phenomenon such as the color of the sky. During the day particles in the atmosphere scatter shorter wavelengths (red) of light more than longer wavelengths (blue) which is what gives the sky its color.[15]

Light moves through materials differently depending upon their refractive index which determines the amount of light that may be reflected when reaching the interface of 2 materials and the critical angle for internal reflection. The refractive index of materials can also vary with the wavelength and frequency of light which is known as dispersion. Dispersion causes white light to divide into its spectral colors. By using the total internal reflection, light can be trapped inside the material (polystyrene, silica, etc.) as it is able to make multiple passes and increasing the optical path length of the photons.

Light waves may also have resonances which result in the absorption of the light of frequency. When no resonance is present, the light is transmitted through the object. There are different types of resonance modes such as whispering gallery mode. Whispering gallery mode refers to the way in which a wave can travel around a concave structure (spheres, domes, etc.) and the original principle is based off how sound waves travelled in the whispering gallery of a cathedral.[16] There are different ways to trap light using different structures and materials to aid in increasing the absorption of photons into a thin film semiconductor.[17] Included are three different types of photonic light trapping schemes (photonic crystals, rough/textured surfaces, and ordered sphere layers).

Photonic crystals are multidimensional periodic artificially created structures that are known for a forbidden electromagnetic bandgap. In a photonic band gap, the electromagnetic density of states is zero which inhibits spontaneous emission. An example of a photonic crystal is shown in Figure 3.3a. The periodicity of a photonic crystal can aid in light scattering for the

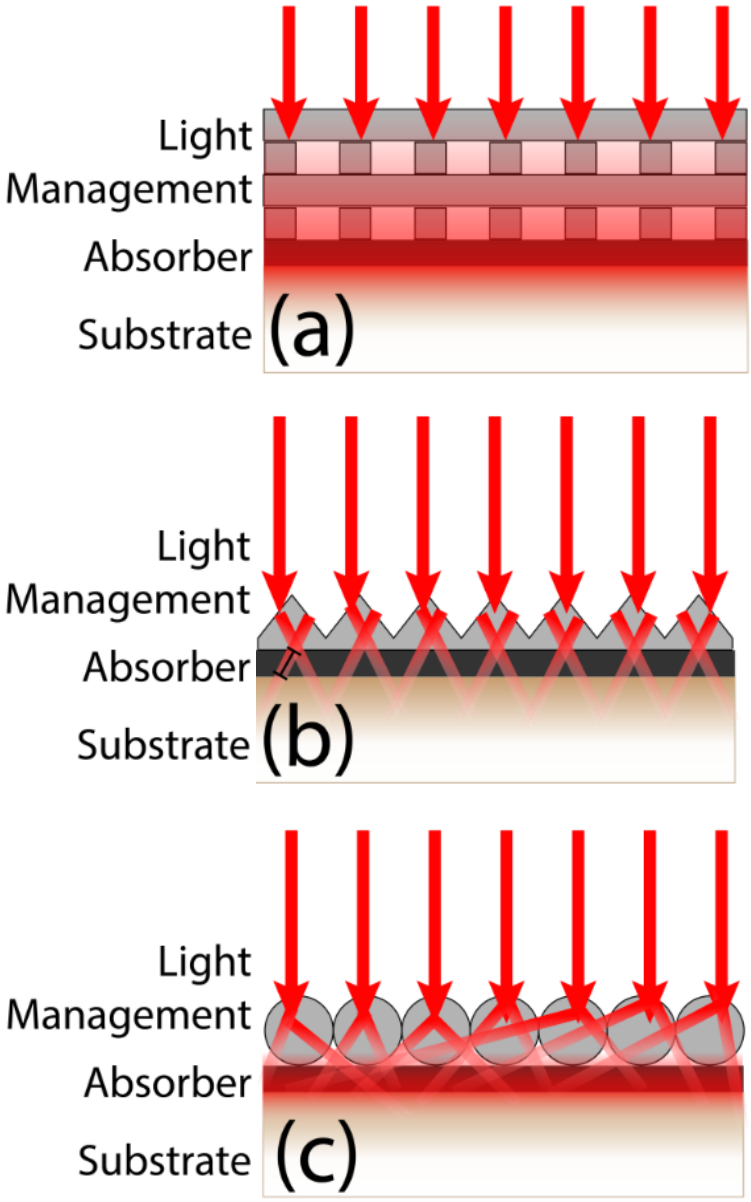

Figure 3.3 Schematic representation of photonic crystals (a), rough/textured surface (b), and ordered sphere layer (c).

prevention of light being trapped internally in a semiconductor layer due to total internal reflection.[18,19] While this may be useful for particular wavelengths, it is also a hinderance because light propagation is essentially forbidden in certain frequencies due to the photonic band gap. In the article by Nirmal et al, they use a mold constructed from polydimethylsiloxane to template ZnO patterned photonic crystals onto a layer of ZnO.[20]

The process of creating the ZnO photonic crystal patterned layer started with the creation of the polydimethylsiloxane mold that will later template the patterned structure using a silicon master template. The formation of the ZnO photonic crystal structure was done on an indium tin oxide (ITO) substrate. A ZnO precursor solution was made using zinc acetate and diethanolamine and then deposited onto the surface ensuring full coverage. The polydimethylsiloxane mold with photonic crystal structure was placed on the precursor coated substrate and firmly held in place while the structure was annealed via a hot plate. Once the patterned ZnO photonic crystal layer was successfully transferred the mold is peeled away leaving behind the patterned ZnO photonic crystal.[20]

A different approach to take for the light trapping structure is roughened or textured surfaces with an example shown in Figure 3.3b. For textured or roughened surfaces, there advantages to this technique. By developing the surface structure, a reduction in surface reflection can occur. Another effect that occurs is an increase in the optical path length caused by diffraction and the enhancement of internal reflection which reduces the amount of light that escapes.[21] Some processes to create a textured surface will give nonreproducible surfaces due to the random nature of the process. One of those processes includes chemical etching. Chemical etching uses specific chemicals to erode the material.

In the article by M. van Eerden et al, a diluted $NaOH/H_2O_2$ etchant solution is used to texture the surface of $Al_{0.3}Ga_{0.7}As$. The etchant solution consisted of 0.12M NaOH and 0.39M of H_2O_2. With a chemical etching technique, control over the texturization of the surface is difficult. The rate of etching slows due to an increase in reaction products not diffusing throughout the solution if no solution agitation occurs. Having substantial control over the rate of etching will vary which is dependent upon how much of the $NaOH/H_2O_2$ solution is able to contact with the surface. The initial etch rate determined by this process was approximately 600nm/min within the first few seconds. However, the etch rate drops significantly to below 100nm/min when no agitation of the solution is done. The amount of chemical etchant may vary in concentration across the surface throughout the process which leads to portions of the surface being etched away more than others. With an inconsistent surface etching, this may lead to variation of the surface across samples or devices.[22] Having rational control of the chemical etchant process may not be achievable due to inconsistent results across multiple samples. While this may be a problem, the roughened or textured surfaces created are still capable of scattering light into nonnormal propagation.

The final approach shown in Figure 3.3c is the use of an ordered sphere layer. Ordered sphere layers can be created through many different methods. Some of these methods include electrophoretic deposition, spin coating, and slow evaporation to coat the surface of a substrate with nanospheres. Electrophoretic deposition is the process which uses charged particles in a colloidal suspension to deposit the colloids onto the surface of a conductive substrate. Spin coating is the process in which a solution of choice is deposited onto the substrate surface and then spun into a thin layer on the surface at a high rate of speed. Slow evaporation is the process in which low concentration colloidal suspensions are placed into a heated environment to induce

evaporation of the solvent so that the colloids are deposited onto the substrate. Each of these processes require different materials and equipment to obtain the deposition of an ordered sphere layer.

The spheres used for this approach are created through a process developed by Stöber et al in which the creation of silica spheres was done.[23] The process was later researched further in order to control the size and mass fraction of the fabricated spheres by Bogush et al.[24] The silica spheres were created in a reaction vessel that was placed into a constant temperature bath. A solution of ammonia saturated ethanol is created by passing concentrated ammonia through a drying column and subsequently bubbling it through ethanol. This solution along with ethanol, ammonium hydroxide, deionized water is added into the reaction vessel. Once the solution comes to temperature, tetraethyl orthosilicate is added into the reaction vessel quickly while the solution is being stirred.[23,24]

The ordered sphere layer is a combination of the two previous approaches due to the light scattering capabilities, but also having resonant propagation and concentration of light near the thin absorber layer. The spheres typically will have a diameter in the range of micro to nanometer. The diameter of the colloids is proportional to the wavelength of light The diameter of the colloids will cause reflection of a particular wavelength to be reflected instead of absorbed. The spheres self-assemble into hexagonally close packed layer on the surface of the thin film semiconductor. By controlling the diameter of the spheres, an increase the absorbed photons can be obtained. Controlling the diameter of the spheres cannot be actively done during the deposition process. The change in diameter must be done between samples to determine which diameter increases the photon absorption the most. This light trapping scheme has the most tunability of the three processes. The tunability allows for multiple parameters to be

adjusted in between samples to optimize the absorption of light into the semiconductor layer. The parameters that can be adjusted are changing the sphere diameter, number of layers (single or multiple layers), and the material of the sphere layer can be changed to increase the absorption that can be individually tailored to different materials or applications.[25]

3.4: Colloidal Self-Assembly Techniques

Micron- to nanometer-diameter spheres (also known as colloids) can be deposited through self-assembly techniques onto substrates. Self-assembly takes place in a colloidal suspension when the spheres forming the colloidal layer move in subject to the constraints of the system they are placed in. The system allows for a stimulant to aid in the assembly to obtain the desired colloidal layer.[26] Some of these techniques are electrophoretic deposition, spin coating, and slow evaporation.[27] While each technique has advantages of coating substrates, choosing the best technique requires an understanding of how each one works with any potential disadvantages.

Electrophoretic deposition is a process where charged particles attach to the oppositely charged surface upon application of an electric field. There are two different types of electrophoretic deposition that allows for a specific electrode to be coated as the deposition occurs. Anodic deposition is the process where negatively charged particles are deposited onto the anode as shown in Figure 3.4a. Cathodic deposition is when positively charged particles are deposited onto the cathode as shown in Figure 3.4b. The principle driving force of this process is the charge on the particle and the electrophoretic mobility of the particles in a solvent under the influence of an applied electric field.

There are two different types of stabilizations for colloids in suspension: electrostatic and steric stabilization.[28] Electrostatic stabilization is the attractive van der Waals forces that are counterbalanced via replusive coulomb forces that act between the charged colloidal spheres. Steric stabilization embraces aspects of the stabilization of colloidal spheres through nonionic macromolecules.[29] A schematic representation of this can be found in Figure 3.5.[28]

A conductive substrate must be used in order for the surface to be deposited onto with colloids. Some examples of substrates that would not need coated to become conductive are indium tin oxide (ITO) or fluorine-doped tin oxide (FTO) glass substrates. These substrates are able to support deposition from auqeous ethanol colloidal solutions containing submicrometer-sized charged spheres.[28] In the article by Rogach et al, a technique using electrophoretic deposition was developed to deposit a three-dimensional colloidal crystal using polystyrene latex spheres suspended in aqueous ethanol. The polystyrene spheres used had carboxyl and sulfate groups attached to the surface of the spheres.

The electrophoretic deposition process of the polystyrene spheres was done using the ITO substrate as the anode and a stainless steel sheet as the counter electrode. The electrodes were placed 0.5cm apart and fixed to be in parallel to each other. The counter electrode was connected to a direct current power supply via an ammeter. The colloidal suspension of 1% polystyrene spheres was mixed with 30% aqueous NH_4OH solution in an ultrasonic water bath. 2mL of ethanol was also added to bring the final concentration to 0.33% A constant voltage of 2V is applied to the ITO anode substrate for 30 minutes for the deposition of the negatively charged polystyrene spheres to occur.[30]

While the approach used by Rogach et al may have used ethanol in the colloidal suspension, other solvents with high dielectric constants may be used as well.[30] Some of these

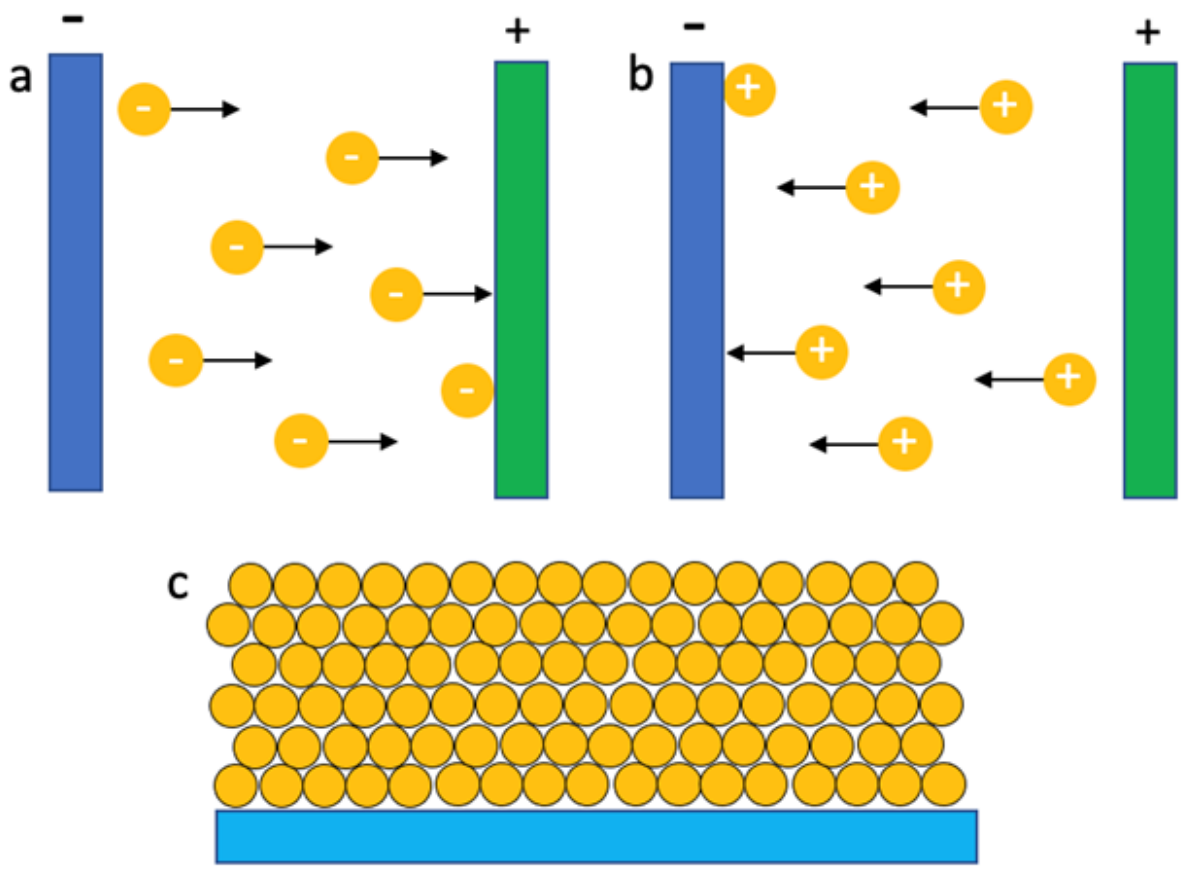

Figure 3.4 Electrophoretic deposition: (a) shows the process of a cathodic deposition, (b) shows anodic deposition, and (c) shows an example of a 3-dimensional colloidal structure.

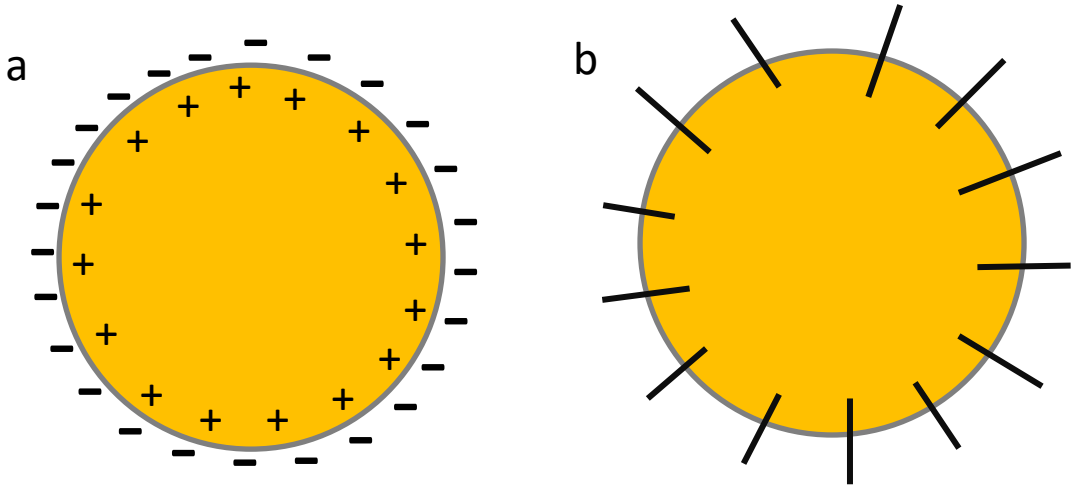

Figure 3.5 Schematic illustration of electrostatic (a) and steric (b) stabilization of colloidal suspensions.

solvents include methanol, n-propanol, iso-propnaol, n-butanol, ethylene glycol, acetone, and acetylacetone. An increase in the conductivity is noticed when the dielectric constant of the solvent increases but, if the conductivity of the solution becomes too high the particle motion becomes very low. When there is a solvent present with too low of a dielectric constant, the deposition process may fail to occur due to an insufficient dissociative power. Higher dielectric constants have a high ionic concentration in the liquid that aids in the reduction in size of the double layer region and the electrophoretic mobility.[28]

This method is a versatile and simple approach to creating colloidal layers with highly crystalline structure. The thickness and morphology of the deposited nanostructure can be controlled through adjustments of the deposition time and applied potential. Due to the applied potential, the colloids used must be constructed from a material that has a charge, like silica or polystyrene with additional surface groups attached, which limits what materials that may be used.[28,30] Also, electrophoretic deposition is best suited for the creation of a multilayered three-dimensional structure as shown in Figure 3.4c and not for smaller two-dimensional structures.[28]

Another technique that can be used to create colloidal layers is through spin coating. Spin coating is the process in which the solution of choice is deposited and then spun into a thin layer on a substrate's surface at high rates of speed. Well-ordered sphere layers can be obtained through attractive capillary forces and subsequent crystal growth driven by convective particle flux caused by the evaporation of water from ordered crystalline regions.[31] Capillary forces is the process of a liquid flowing through narrow spaces without assistance of, or even in opposition to, any external forces (like gravity). Cohesive forces between liquid molecules are balanced and shared with all neighboring molecules except at the surface of the liquid. At the surface of the liquid, the spheres are not equally surrounded by liquid molecules on all sides causing an

exertion of stronger attractive forces to occur on or near the surface. Surface tension is an imbalance in the attractive forces between molecules and can be related to the decrease in surface energy because of a decrease in surface area.[32]

One mechanism that is predominate with the spin coating method is the “coffee ring effect”. This effect is caused when some particles irreversibly stick to a substrate during the initial drop of the suspension at the periphery under action of capillary forces by pinning the contact line and resulting in evaporation from the edge being compensated from the interior flow. This action ultimately pulls suspended particles to the drop periphery and subsequently develops a ring of particles.[31]

Most spin coaters can reach speeds from 50 revolutions per minute (rpm) to upwards of 10,000 rpm.[31] The process of spin coating is a 4-step process as shown in Figure 3.6. The first step is the deposition of solution onto the substrate surface before starting the spin coater. Once started the spin coater causes the solution to even out across the surface which allows the evaporation process to occur. The solvent will either evaporate off the surface or be flung off, leaving behind the colloids on the surface. If any residual solution is left, then the remaining will be spun off the surface via the spin off final step.[33]

For the process of spin coating a colloidal suspension onto a sample to be effective, dispersion properties such as particle weight fraction, solvent volatility, and viscosity should be considered. There are steps that can be taken to minimize these effects and achieve better surface coverage. To aid with viscosity of the suspension, a surfactant solution is used to decrease surface tension so that the surface is only coated in the colloids. By lessening the surface tension, fluid thinning occurs due to both shear forces and the evaporation of solution. The surfactant can

also aid with the volatility of the solution due to most surfactant solutions containing a component that is highly volatile (methanol or ethanol).[31]

The final technique that could potentially be used for colloidal self-assembly is slow evaporation. Slow evaporation is the process where a low concentration colloidal suspension is placed into a heated environment to induce the evaporation of the solvent to deposit the colloids onto the substrate. As shown in Figure 3.7 from Ling Li et al from reference [34],[34] the spheres in the solution will come to the surface of the solution.[35] Typically, the substrate is immersed vertically or at an angle into a colloidal suspension, the colloidal particles are driven to the meniscus of the solution by the evaporation-induced fluid flow. When the colloids reach the meniscus, they are brought to the surface of the substrate and adhere to the surface as the solution evaporates.[34] This set up is placed into an incubator to maintain a constant temperature. Depending on the solution components, the temperature may change slightly to obtain a uniform coating. With a suspension containing just water and the colloids, the ideal temperature stays around 45 to 50°C while a suspension containing a volatile chemical (such as methanol or ethanol) an adjustment to the temperature would need to be done.

Due to the process of evaporation in this technique, there are many factors that the deposition is sensitive to when changes occur. These factors include effective particle interactions, evaporation rate as controlled by temperature, pressure, relative humidity, and the solvent's properties.[36] Temperature and pressure can cause areas in which no colloids are present on the surface. If the evaporation process occurs too quickly, many areas without colloids will appear which makes a nonuniform and inconsistent coating on the substrate. If a suspension of water and colloids is placed into an incubator at 50°C and atmospheric pressure, the deposition will take approximately 48 to 60 hours. The relative humidity in the incubator can also slow

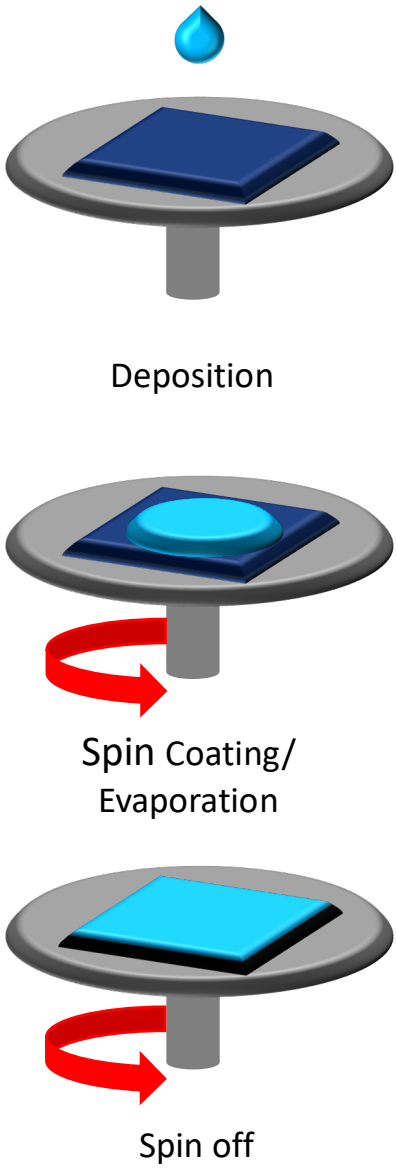

Figure 3.6 Schematic representation of the 4-step process for spin coating: deposition, spin coating, evaporation, and spin off.

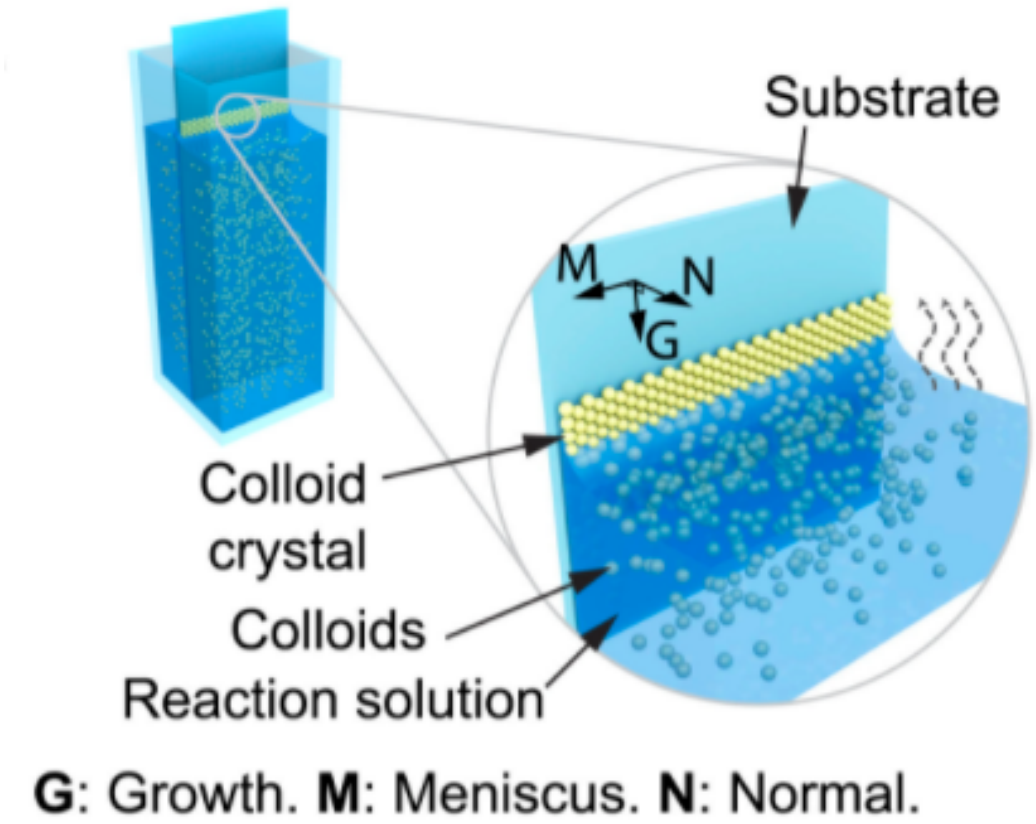

Figure 3.7 Schematic representation of the slow evaporation process during deposition. (Reprinted with permission from reference 34. Copyright © 2021 PNAS)

down the evaporation process of the solvent as the higher humidity causes evaporation to slow due to the amount of moisture present in the air. Uniform and minimal defect coatings are achieved when drying is sufficiently fast to increase local particle density yet still slow enough that the diffusion can anneal defects before additional grain boundaries or layers form.[35]

In comparison to the two previously mentioned techniques, the slow evaporation method would by far take the longest due to the nature of evaporation depending on types of solvents present and temperature at which the process is exposed to. However, the technique can be adjusted (concentration of suspension, temperature, etc.) for any number of layers desired with consistent results. By adjusting the concentration of the colloidal suspension, the range in number of layers can extend from just a monolayer to a large three-dimensional structure. A more concentrated suspension will deposit multiple layers while lower concentrations of spheres will fewer layers or a monolayer of colloids. Adjusting the temperature from 50 to 45°C on the same solution concentration can also increase the number of layers, but less of the overall surface may be coated. Unlike spin coating and electrophoretic deposition, a small container to hold the samples and colloidal suspensions while drying can easily hold multiple samples at a time even with the larger time frame. With the other techniques, unless there are multiple set ups, typically only one sample can be created at a time.[36] A comparison of the three techniques stating the advantages and disadvantages can be found in Table 3.1.

Table 3.1 Comparison of electrophoretic deposition, spin coating, and slow evaporation

Deposition Method	Pros	Cons
Electrophoretic Deposition	Quick deposition process Constructs 3-dimensional colloidal structure	Not suitable for monolayers Particles must have a charge May obtain coating within 30 minutes
Spin Coating	Quick deposition process Able to construct mono- or bi-layers	Requires an extensive cleaning process Only complete one sample at a time Requires extensive testing to determine optimal speeds
Slow Evaporation	Consistent coatings across multiple samples Coat multiple samples at a time Suitable for mono or multiple layers	Takes multiple days to obtain coatings

References

(1) Burford, N. M.; El-Shenawee, M. O. Review of terahertz photoconductive antenna technology. *Optical Engineering* **2017**, *56* (1), 010901.

(2) Kawano, Y. 13 - Terahertz nano-devices and nano-systems. In *Handbook of Terahertz Technology for Imaging, Sensing and Communications*, Saeedkia, D. Ed.; Woodhead Publishing, 2013; pp 403-422.

(3) Yu, C.; Fan, S.; Sun, Y.; Pickwell-Macpherson, E. The potential of terahertz imaging for cancer diagnosis: A review of investigations to date. *Quantitative imaging in medicine and surgery* **2012**, *2* (1), 33-45. DOI: 10.3978/j.issn.2223-4292.2012.01.04 PubMed.

(4) Xie, J.; Ye, W.; Zhou, L.; Guo, X.; Zang, X.; Chen, L.; Zhu, Y. A Review on Terahertz Technologies Accelerated by Silicon Photonics. *Nanomaterials* **2021**, *11* (7). DOI: 10.3390/nano11071646.

(5) Chuang, S. L. *Physics of photonic devices*; John Wiley & Sons, 2012.

(6) Gupta, S.; Frankel, M. Y.; Valdmanis, J. A.; Whitaker, J. F.; Mourou, G. A.; Smith, F. W.; Calawa, A. R. Subpicosecond carrier lifetime in GaAs grown by molecular beam epitaxy at low temperatures. *Applied Physics Letters* **1991**, *59* (25), 3276-3278. DOI: 10.1063/1.105729.

(7) Batista, J. S.; Churchill, H. O. H.; El-Shenawee, M. Black phosphorus photoconductive terahertz antenna: 3D modeling and experimental reference comparison. *Journal of the Optical Society of America B* **2021**, *38* (4), 1367-1379. DOI: 10.1364/JOSAB.419996.

(8) Maier, S. A.; Brongersma, M. L.; Kik, P. G.; Meltzer, S.; Requicha, A. A. G.; Atwater, H. A. Plasmonics—A Route to Nanoscale Optical Devices. *Advanced Materials* **2001**, *13* (19), 1501-1505, https://doi.org/10.1002/1521-4095(200110)13:19. DOI: https://doi.org/10.1002/1521-4095(200110)13:19 (acccessed 2022/02/24).

(9) Barnes, W. L. Surface plasmon–polariton length scales: a route to sub-wavelength optics. *Journal of Optics A: Pure and Applied Optics* **2006**, *8* (4), S87-S93. DOI: 10.1088/1464-4258/8/4/s06.

(10) Burford, N. M.; Evans, M. J.; El-Shenawee, M. O. Plasmonic Nanodisk Thin-Film Terahertz Photoconductive Antenna. *IEEE Transactions on Terahertz Science and Technology* **2018**, *8* (2), 237-247. DOI: 10.1109/TTHZ.2017.2782484.

(11) Arthur, J. R. Molecular beam epitaxy. *Surface Science* **2002**, *500* (1), 189-217. DOI: https://doi.org/10.1016/S0039-6028(01)01525-4.

(12) Bhattacharjee, P. R. The generalized vectorial laws of reflection and refraction. *European Journal of Physics* **2005**, *26* (5), 901-911. DOI: 10.1088/0143-0807/26/5/022.

(13) Drosdoff, D.; Widom, A. Snell's law from an elementary particle viewpoint. *American Journal of Physics* **2005**, *73* (10), 973-975. DOI: 10.1119/1.2000974 (acccessed 2021/02/26).

(14) Kerker, M. *The scattering of light and other electromagnetic radiation: physical chemistry: a series of monographs*; Academic press, 2013.

(15) Hulst, H. C.; van de Hulst, H. C. *Light scattering by small particles*; Courier Corporation, 1981.

(16) Chiasera, A.; Dumeige, Y.; Féron, P.; Ferrari, M.; Jestin, Y.; Nunzi Conti, G.; Pelli, S.; Soria, S.; Righini, G. C. Spherical whispering-gallery-mode microresonators. *Laser & Photonics Reviews* **2010**, *4* (3), 457-482, https://doi.org/10.1002/lpor.200910016. DOI: https://doi.org/10.1002/lpor.200910016 (acccessed 2022/03/30).

(17) Khan, M.; Xufeng, W.; Bermel, P.; Alam, M. Enhanced light trapping in solar cells with a meta-mirror following generalized Snell's law. *Optics Express* **2014**, *22*. DOI: 10.1364/OE.22.00A973.

(18) Boroditsky, M.; Vrijen, R.; Krauss, T. F.; Coccioli, R.; Bhat, R.; Yablonovitch, E. Spontaneous emission extraction and Purcell enhancement from thin-film 2-D photonic crystals. *Journal of Lightwave Technology* **1999**, *17* (11), 2096-2112. DOI: 10.1109/50.803000.

(19) John, S.; Wang, J. Quantum electrodynamics near a photonic band gap: Photon bound states and dressed atoms. *Physical Review Letters* **1990**, *64* (20), 2418-2421. DOI: 10.1103/PhysRevLett.64.2418.

(20) Nirmal, A.; Kyaw, A. K. K.; Jianxiong, W.; Dev, K.; Sun, X.; Demir, H. V. Light Trapping in Inverted Organic Photovoltaics With Nanoimprinted ZnO Photonic Crystals. *IEEE Journal of Photovoltaics* **2017**, *7* (2), 545-549. DOI: 10.1109/JPHOTOV.2017.2650560.

(21) Sai, H.; Kanamori, Y.; Arafune, K.; Ohshita, Y.; Yamaguchi, M. Light trapping effect of submicron surface textures in crystalline Si solar cells. *Progress in Photovoltaics: Research and Applications* **2007**, *15* (5), 415-423. DOI: https://doi.org/10.1002/pip.754.

(22) van Eerden, M.; Bauhuis, G. J.; Mulder, P.; Gruginskie, N.; Passoni, M.; Andreani, L. C.; Vlieg, E.; Schermer, J. J. A facile light-trapping approach for ultrathin GaAs solar cells using wet chemical etching. *Progress in Photovoltaics: Research and Applications* **2020**, *28* (3), 200-209. DOI: https://doi.org/10.1002/pip.3220.

(23) Stöber, W.; Fink, A.; Bohn, E. Controlled growth of monodisperse silica spheres in the micron size range. *Journal of colloid and interface science* **1968**, *26* (1), 62-69.

(24) Bogush, G. H.; Tracy, M. A.; Zukoski Iv, C. F. Preparation of monodisperse silica particles: control of size and mass fraction. *Journal of non-crystalline solids* **1988**, *104* (1), 95-106.

(25) Grandidier, J.; Callahan, D. M.; Munday, J. N.; Atwater, H. A. Light Absorption Enhancement in Thin-Film Solar Cells Using Whispering Gallery Modes in Dielectric Nanospheres. *Advanced Materials* **2011**, *23* (10), 1272-1276, https://doi.org/10.1002/adma.201004393. DOI: https://doi.org/10.1002/adma.201004393 (acccessed 2021/02/20).

(26) Galisteo-López, J. F.; Ibisate, M.; Sapienza, R.; Froufe-Pérez, L. S.; Blanco, Á.; López, C. Self-Assembled Photonic Structures. *Advanced Materials* **2011**, *23* (1), 30-69. DOI: https://doi.org/10.1002/adma.201000356.

(27) Chandramohan, A.; Sibirev, N. V.; Dubrovskii, V. G.; Petty, M. C.; Gallant, A. J.; Zeze, D. A. Model for large-area monolayer coverage of polystyrene nanospheres by spin coating. *Scientific reports* **2017**, *7* (1), 1-8.

(28) Besra, L.; Liu, M. A review on fundamentals and applications of electrophoretic deposition (EPD). *Progress in materials science* **2007**, *52* (1), 1-61.

(29) Mo, S.; Shao, X.; Chen, Y.; Cheng, Z. Increasing entropy for colloidal stabilization. *Scientific Reports* **2016**, *6* (1), 36836. DOI: 10.1038/srep36836.

(30) Rogach, A. L.; Kotov, N. A.; Koktysh, D. S.; Ostrander, J. W.; Ragoisha, G. A. Electrophoretic Deposition of Latex-Based 3D Colloidal Photonic Crystals: A Technique for Rapid Production of High-Quality Opals. *Chemistry of Materials* **2000**, *12* (9), 2721-2726. DOI: 10.1021/cm000274l.

(31) Toolan, D. T. W.; Fujii, S.; Ebbens, S. J.; Nakamura, Y.; Howse, J. R. On the mechanisms of colloidal self-assembly during spin-coating. *Soft Matter* **2014**, *10* (44), 8804-8812.

(32) Lamkin-Kennard, K. A.; Popovic, M. B. 8 - Molecular and Cellular Level—Applications in Biotechnology and Medicine Addressing Molecular and Cellular Level. In *Biomechatronics*, Popovic, M. B. Ed.; Academic Press, 2019; pp 201-233.

(33) Park, B.; Na, S. Y.; Bae, I.-G. Uniform two-dimensional crystals of polystyrene nanospheres fabricated by a surfactant-assisted spin-coating method with polyoxyethylene tridecyl ether. *Scientific reports* **2019**, *9* (1), 1-9.

(34) Li, L.; Goodrich, C.; Yang, H.; Phillips, K. R.; Jia, Z.; Chen, H.; Wang, L.; Zhong, J.; Liu, A.; Lu, J.; et al. Microscopic origins of the crystallographically preferred growth in evaporation-induced colloidal crystals. *Proceedings of the National Academy of Sciences* **2021**, *118* (32), e2107588118. DOI: doi:10.1073/pnas.2107588118.

(35) Im, S. H.; Park, O. O. Effect of Evaporation Temperature on the Quality of Colloidal Crystals at the Water−Air Interface. *Langmuir* **2002**, *18* (25), 9642-9646. DOI: 10.1021/la025888e.

(36) Howard, M. P.; Reinhart, W. F.; Sanyal, T.; Shell, M. S.; Nikoubashman, A.; Panagiotopoulos, A. Z. Evaporation-induced assembly of colloidal crystals. The Journal of Chemical Physics: 2018; Vol. 149, p 094901.

Chapter 4: Development of a novel black TiO_2 thin film absorber with colloidal monolayer

With the implementation of black phosphorus in the THz device, there is a need for a similar thin film. Black phosphorus has one major limiting disadvantage to be readily used to obtain absorption measurements which is that it is oxidized by oxygen and water in the air.[1] Besides black phosphorus oxidizing when exposed to air, determining any increase in absorption of light in the device is not easily done. With the device being constructed on a Si substrate, the only measurement that could be achieved is reflection of the device. To combat these issues, the thin film must be placed on a substrate that is optically transparent in the visible and infrared light regions. The thin film that is chosen must be developed using a technique or method that allows for control over the thickness of the layer. The thin film layer chosen is a 'black' TiO_2.

The 'black' TiO_2 thin film can be created using an atomic layer deposition (ALD) instrument, but at temperatures that better coincide with chemical vapor deposition. Control over the thickness of the film is achieved by using the ALD. The 'black' TiO_2 thin film will act as a thin film absorber which will aid in the determination of the increase in absorption a monolayer of colloids could potentially give. The monolayer of colloids will be deposited ultimately using the slow evaporation method.

Using a UV-Vis Spectrometer, reflectance and transmission measurements can be obtained to determine the absorption values of the 'black' TiO_2 layer with and without a monolayer of colloids. Using the reflectance and transmission measurements, the absorption can be determined using:

$$A\% = 100 - \%T - \%R \qquad \text{(Equation 1)}$$

Where A is the absorbance, T is transmittance, and R is reflectance. The goal is to see how much of an increase in absorption the colloids may allow. While it is expected for an increase in the

absorption to occur, certain wavelengths that coincide with the diameter of the colloids, may have more reflection occur due to the opalescent bands. Opalescence is a milky iridescent appearance of a dense transparent medium that when illuminated by visible radiation, such as sunlight, causes a higher reflection of light to occur at these opalescent bands. Natural occurring examples of opalescence are exhibited in butterflies, chameleons, marine creatures, and even in flora.[2] When this phenomenon occurs, the thin film would be better off without the colloidal layer as there is no benefit to having the spheres present. However, having an overall increase in the absorption would mean that the colloidal layer could potentially increase the absorption in the THz device. Increasing the absorption in the THz device would, in turn, create a stronger THz emission.

4.1: Deposition of the 'Black' TiO_2 Thin Film

Atomic layer deposition (ALD) is a thin film deposition technique that is based on the sequential use of materials in the gas-phase of a chemical process using chemical precursors. An example of an ALD process was used from reference [3] by Reed et al. In this article, a TiO_2 layer was synthesized using tetrakis(dimethylamido)titanium (TDMAT) and H_2O. The reactor chamber was set to 150°C and the TDMAT precursor cylinder was heated to 80°C during the process. The H_2O was set at room temperature. During the entire deposition, the mass flow control of the nitrogen carrier gas was set to 20 sccm. Each cycle consisted of pulses of the TDMAT (100ms, purge of 15s) and H_2O (15ms, purge of 25s). This cycle was repeated until desired thickness was achieved.[3] A schematic representation of this process is shown in Figure 4.1 from the article reference [4] by Steven George. There are many advantages to using ALD

for thin film development. ALD can be used to deposit films with precise control, even down to a thickness of a few nanometers.[4]

Before coating a substrate surface using ALD, the substrate must be cleaned of any organics or other particles. This cleaning process is done to ensure the desired surface for coating so that the coating is uniform and prevents defects to form. The cleaning process for the substrate (quartz) included a four-step rinse and a short period in a UV-ozone cleaner. The quartz was rinsed in order by acetone, methanol, isopropanol, and deionized water. Once rinsed with the solutions, the substrates were patted dry using a Kimwipe and then placed into the UV-ozone cleaner for 15 minutes. Once the cleaning process is completed, the quartz is ready to be coated.

While the ALD is used to deposit the 'black' TiO_2 layer, it is important to note that the temperature at which the reaction is done is more of a chemical vapor deposition process. Chemical vapor deposition is the process in which gas phase molecules are decomposed in some manner which leave behind solid materials and is typically done at high temperatures.[5] With the chamber and door heat of the ALD chamber being set to high temperatures (300°C), the precursors are decomposed instead of having surface site reactions. The ALD is also able to keep the environment of the reaction chamber under nitrogen flow. The nitrogen environment will aid in the TiO_2 film having the black color instead of a transparent purple hue that TiO_2 typically has.

The creation of the 'black' TiO_2 layer is done by placing the quartz onto an aluminum bar on the ALD platform. The chamber and door heat are set to 300°C for this process and the tetrakis(dimethylamino)titanium (TDMAT) precursor bottle is set to 70°C before the start of the run. Each cycle of 'black' TiO_2 consisted of an exposure to the precursor pulse TDMAT (100ms,

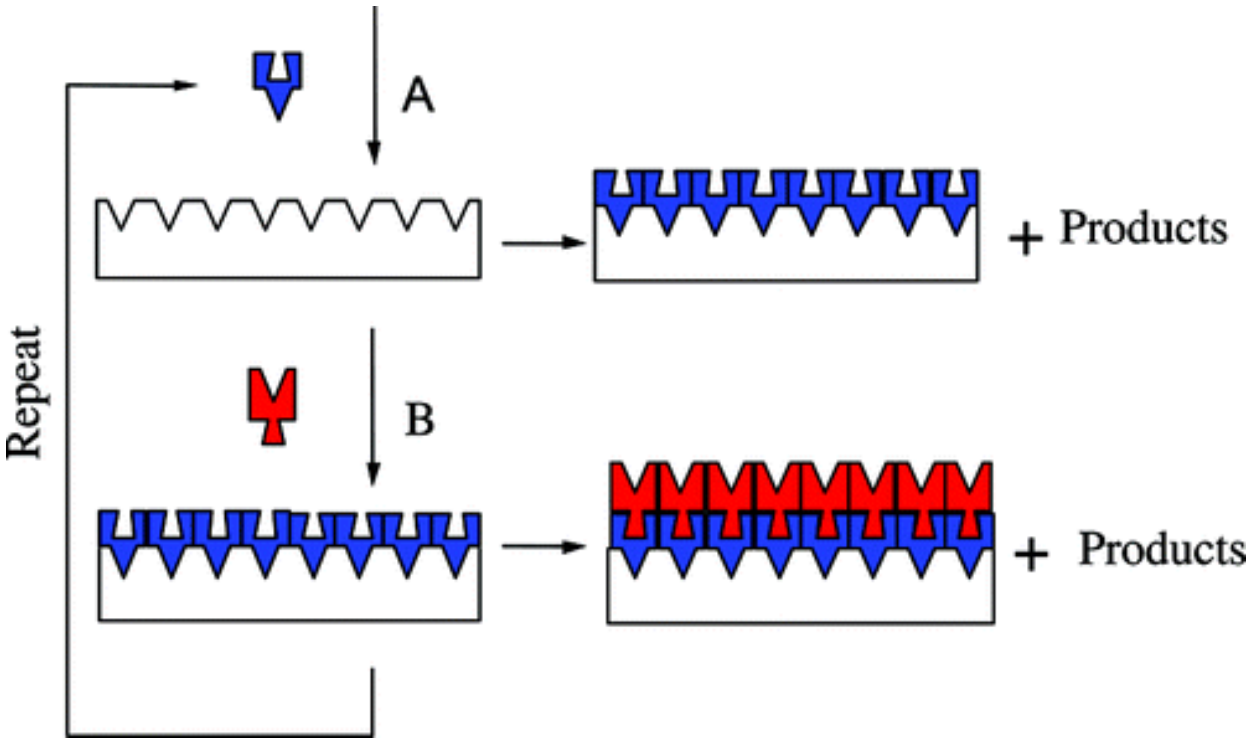

Figure 4.1 Schematic illustration of a two reactant ALD process for coating a substrate. (Reprinted with permission from reference 4. Copyright © 2009 American Chemical Society)

20sccm N_2 carrier gas flow) and a purge step (45s, 100sccm N_2). This cycle was repeated 1200 times.

4.2: Self-assembly of colloidal layer

The self-assembly technique of the colloidal layer was first developed before deposition onto the 'black' TiO_2 thin films could occur. The target uniform coating desired is a monolayer of the colloids. The 'black' TiO_2 thin film was used to aid in measuring the increase of light absorption the colloids could potentially bring when deposited onto the THz device. The process used to deposit the colloids also would need to be capable of coating different materials. Due to the THz device construction, the technique used must be capable of coating a surface without the need for extensive and potentially damaging cleaning methods. Two different methods were tested to determine which technique would be most beneficial in obtaining a uniform monolayer of colloids consistently across multiple samples while not requiring a cleaning process that could potentially damage the THz device.

The first method used for the self-assembly of the monolayer of colloids was spin coating. Spin coating is the process in which a solution of choice is placed onto the substrate and then spun at various speeds to equally coat the entire surface. This technique requires pinpointing the appropriate rates of speed to spin the substrate at for a uniform coating. This process will be developed with a variety of different diameters using polystyrene nanospheres (Polysciences, Inc.). The diameters used to obtain a coating varied from as small as 200nm up to 3μm with each stock suspension of colloids containing a weight percent concentration of 2.6% in water.

Initially, the substrates used were glass microscope slides that were cut into smaller pieces for the development of the techniques needed for the spin coating process. The use of

microscope slides for actual samples would not work due to the nature of the surface. The surface of the microscope slides has a substantial height variation allowance which causes the spheres to settle in the lower regions of the surface and not be able to overcome the taller regions. An example of a microscope slide sample with 3.0μm polystyrene spheres is shown in Figure 4.2. Instead of a uniform coating being easily obtained across a large portion of the sample, the colloids will settle into the lower regions of the surface and may not cover all the surface. Also, the glass slide is not fully transparent in the UV and visible light regions. Ideally, the best substrate is quartz since it is transparent in both the UV and visible light range and has a more optically flat surface structure with the surface variation being on the nanometer scale or smaller. The clear quartz substrate also allows the absorption of light to obtained in the 'black' TiO_2 layer.

When initially developing the spin coating technique, the glass substrates were rinsed with acetone, methanol, isopropanol, and deionized (DI) water then patted dry with a Kimwipe. Next, the substrates were placed in the UV-ozone cleaner for 30 minutes as this aided in not just cleaning, but also making the surface more hydrophilic. After a few rounds of trials, sonication of the substrates was implemented. This was implemented to aid in the cleanliness of the substrates before the UV-ozone step. The substrates were put into acetone, methanol, isopropanol, and DI water for 15 minutes each to sonicate before being patted dry with a Kimwipe before being placed in the UV-ozone cleaner to finish up the process.

Another treatment process to clean the substrates that is used in other spin coater works, is the following treatment process. The substrate is immersed into an oxidant solution, also known as a piranha solution, containing a mixture of H_2SO_4 and H_2O_2 with a volume ratio of 3 to 1 (v/v) for 1 hour. This was followed by rinsing with DI water. The second part included the

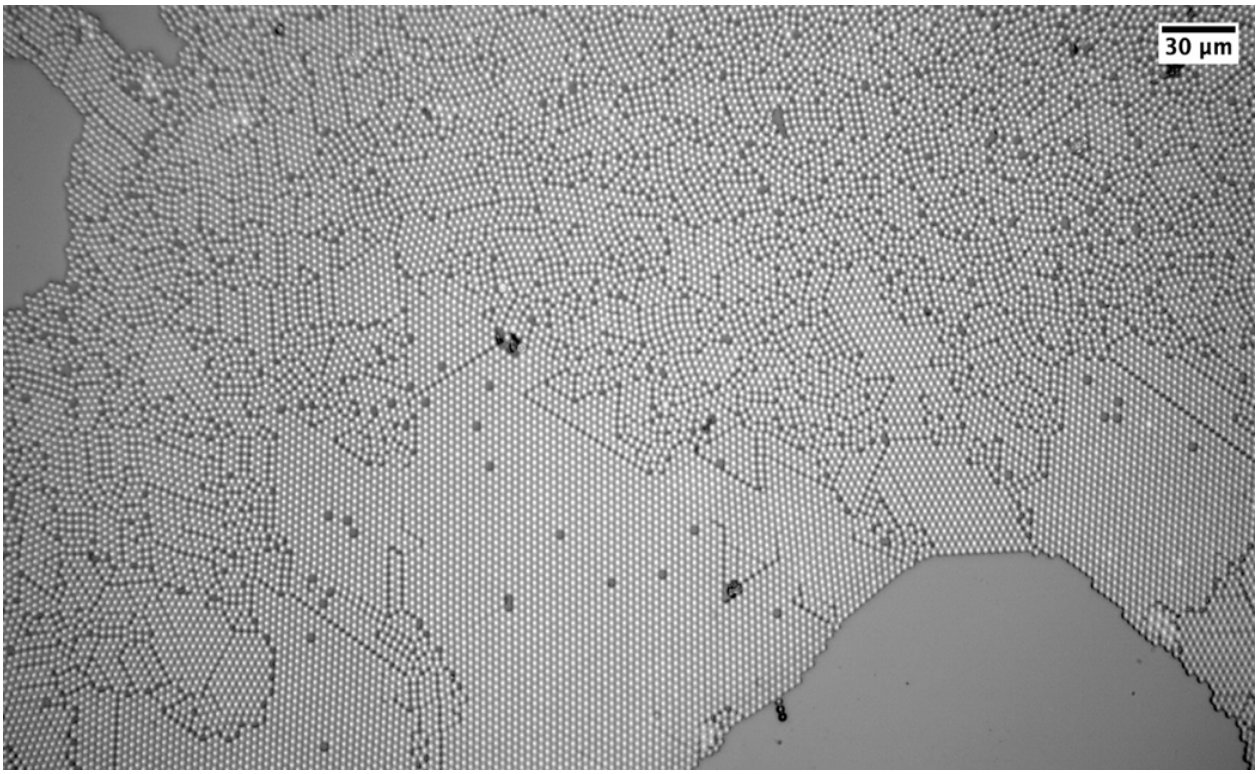

Figure 4.2 3.0µm polystyrene spheres on glass microscope slide coated via spin coating process.

substrate being treated via immersion into a solution of H_2O: NH_4OH: 30% H_2O_2 (5: 1: 1 v/v/v) at 80°C. This was also followed by rinsing with DI water and dried.[6,7] While this process showed favorable results, the device in which the colloids would be coated onto would require the gentler cleaning process that was mentioned previously so that the THz device would not be damaged or have erosion of the electrodes.

While the gentler cleaning process was chosen, another way to aid in a more uniform coating is by using a surfactant. By using a surfactant, the surface tension can be minimized and aide in obtaining a more uniform coating. The surfactant used was Triton X100 in a volumetric ratio of 1:400 of Triton X100 to methanol. There are a few different ways to coat the substrate with both the surfactant solution and colloidal suspension. Both solutions can be individually added in a stepwise manner, or the solutions can be combined and then deposited onto the substrates surface. Regardless of the method used, the outcome for each method gave similar if not identical results.

For example, a 1μm diameter colloidal suspension is added dropwise onto the glass slide using 2-3 drops. When the diameter of the colloids is changed, the number of drops needed will vary due to the weight difference per sphere when the diameter changes. Next, the addition of 4-6 drops of the surfactant solution is added before starting the spin coater. The spin coater speeds varied depending on the diameter of the spheres. Regardless of the spheres, the spin coater would be started out for a lower speed to begin with, typically around 500 revolutions per minute (rpm), for a short period of time before increasing. The increase in speed varied depending on the sphere size, smaller particles would require higher rpms otherwise the solvent stays on the surface. The final speed increase went to around 3200 rpm to spin off any excess remaining solvent on the surface. This process produced a roughly 50% coverage of the glass slide. The

coverage of the slide also gave areas that consisted of multiple layers randomly throughout but were consistently located around the edges of the surface. Besides using the glass slides with a significant height variation allowance, silicon wafers and quartz cut into 1.5 cm by 1.5 cm squares were used. The wafers and quartz have a more optically flat surface than the glass microscope slides and were also included in the process described above. Both types of substrates had slightly better coverage of up to almost 70% coverage at the maximum, but the coverage was still not uniform over large areas across various samples.

Due to the lack of consistent uniform monolayers over a large area, a switch in self-assembly techniques was done. The next technique implemented to obtain the consistent coatings is slow evaporation. The cleaning process of sonication and UV-ozone cleaning of the substrates done with spin coating remained the same. For slow evaporation, the substrates being coated are placed at an acute angle against the side of a plastic scintillation vial as shown in Figure 4.3. The substrates are placed at an acute angle so that as the solvent evaporates, the colloids adhere to the surface well. The diluted colloidal suspension would be added into the vial until the substrate is mostly in the solution, which is approximately 5mL. If the substrate is completely vertical or slides down into a horizontal position during the process, the coatings obtained are not the desired monolayer.

When initially developing this process to obtain a monolayer of colloids, 3 different suspensions at different concentrations for each sphere diameter were created. Each solution would be tested with a silicon wafer and quartz substrates cut into 1.5 cm by 1.5 cm pieces. The suspension that is the closest to coating both substrates with the monolayer would be chosen and adjusted to the appropriate concentration to obtain the monolayer. The temperature at which the vials were under in the incubator's ranged from 45 to 55°C, however the optimal temperature for

Figure 4.3 Glass scintillation vial with a piece of Si wafer angled to show the necessary step up needed for slow evaporation. During actual deposition plastic vials are used instead.

all sphere sizes was found to be 50°C. At this temperature, the solvent takes approximately 2.5 days to dry unless numerous vials with samples are in the incubator at once. The more vials that are present, the more humid the environment can become over time causing the evaporation time to increase and the coatings can subsequently be affected. The samples obtained with slow evaporation overall showed a more consistent deposition process across multiple samples.

Creating the colloidal suspensions with the appropriate concentrations to obtain the monolayer is done via dilution of the stock concentrations. The polystyrene colloids purchased from Polysciences, Inc. that are used for this process all have a stock concentration of 2.6%. Since polystyrene has a density that is similar to water, this concentration can be interpreted as either w/w% or v/v%. For the dilution process, Equation 2 was used to determine the amount of stock solution that would be needed to create the desired suspension concentration:

$$C_1W_1 = C_2W_2 \qquad \text{(Equation 2)}$$

where C is for concentration and W is for weight. The weight can be interchanged for volume as well. The colloidal suspensions created included sphere diameters of 200nm, 350nm, 500nm, 750nm, and 1000nm. Due to the change in diameter size, the concentration must change as well due to the change in the number of spheres that are present in the suspension. Because of the large difference in the concentrations desired from the stock suspensions, a series of dilutions are beneficial. Equation 2 can be used to complete a series of dilutions in order to achieve the final concentration. After several trials of determining the appropriate concentrations, there is a small window in which the concentration of each solution can be slightly higher or lower than the intended concentration and still yield a monolayer of colloids via slow evaporation. This tolerance changes along with the diameter of the colloids and is shown in Table 4.1. The tolerance of concentration allows for a small insufficient or excess mass/volume that is

measured. Table 4.1 shows the various diameters of colloidal suspensions that have been diluted from the stock solutions obtained from Polysciences, Inc. in which a monolayer can be achieved.

Table 4.1 Colloidal suspension concentrations for various sphere diameters. The variation column is the amount of additional change in concentration allowable to still achieve a monolayer.

Sphere Diameter	Concentration (v/v%)	Concentration Tolerance
200nm	0.002%	±0.0002%
350nm	0.0025%	±0.0002%
500nm	0.003%	±0.0003%
750nm	0.005%	±0.0003%
1000nm	0.02%	±0.005%

4.3: Characterization

For the characterization of the black TiO_2 film and colloidal layers, there are several steps that must be taken to get accurate measurements from each sample. Since we are striving for a monolayer of spheres, the use of the optical microscope and scanning electron microscope (SEM) aids in determining the amount of total coverage, the uniformity of coverage, and number of layers present on a sample. The SEM aids in viewing smaller diameter of spheres to fully determine the overall coverage due to the optical microscope only being able to distinctly view spheres with a diameter size of 1 micron or larger. The smaller the diameter becomes, the more difficult viewing the distinct spheres and layers becomes.

The second method used for characterization is UV-Vis spectrometry to obtain reflectance and transmittance measurements to determine absorption using Equation 1. These measurements are done to determine the absorption of the black TiO_2 film before and after the deposition of colloids. By measuring the absorption before depositing the spheres onto the film, we can determine how much of an increase in absorption is obtained for each sphere diameter. This will also aid in determining if there are any prominent resonances that may be specific to a specific sphere diameter.

For the black TiO_2 thin films, the UV-Vis spectrometer was used to determine the percent transmission and reflection measurements of each sample. The measurements can be taken again after each sample is coated with a monolayer of colloids to determine if there are resonances and whether there is an increase in the absorption. To ensure that the colloids do not come off the samples during the measurement process and into the integrating sphere, the use of a plastic washer was implemented. The samples are taped to the washer so that the sample is kept away from the openings of the integrating sphere while measurements are taken. The absorption values

of the colloidal layers will aid in determining how effective the spheres are at increasing the absorption into the 'black' TiO_2 layer. These values will also give information as to the potential absorption increase that can be obtained when the colloids are put onto the THz device. With the THz device not being transparent enough, there is not an effective way to measure the absorbance value difference of the device with and without the colloids.

As shown in Figures 4.4-4.8, there is an overall increase in absorption from approximately 350nm to 1600nm in wavelength. In Figures 4.4-4.6, there is a resonance in which the reflection of the colloids is high and is shown by the arrows. For the 200nm polystyrene (PS) spheres, the increase in reflection is around 475nm, 350nm PS spheres shows an increase in reflection around 815nm, and 500nm PS spheres shows an increase in reflection around 1115nm. At these wavelengths, the 'black' TiO_2 layer would be more efficient without the colloidal layer. Regardless of the diameter size of the spheres, an increase in absorption was noted from approximately 360nm to 1600nm except for the increase in reflection of the 200nm, 350nm, and 500nm spheres. The two peaks at approximately 230nm and 300nm wavelengths across all samples with the colloidal layer are properties of the PS spheres.

After the deposition process of the monolayer of colloids is complete, the samples must be viewed to determine how uniform the coating is. Depending upon the size of colloids used during deposition will depend on what method can suitably view the sphere layer. Particle sizes of 1μm in diameter or larger can be easily viewed using a microscope. Particles of smaller sizes will require the use of a scanning electron microscope (SEM) to differentiate the number of layers or defects of the colloidal coating. To view the samples using the SEM, the polystyrene sphere must be coated with a material that is electrically conductive. The samples shown in Figure 4.9 are two different samples. The sample on the left has a coating of 750nm polystyrene

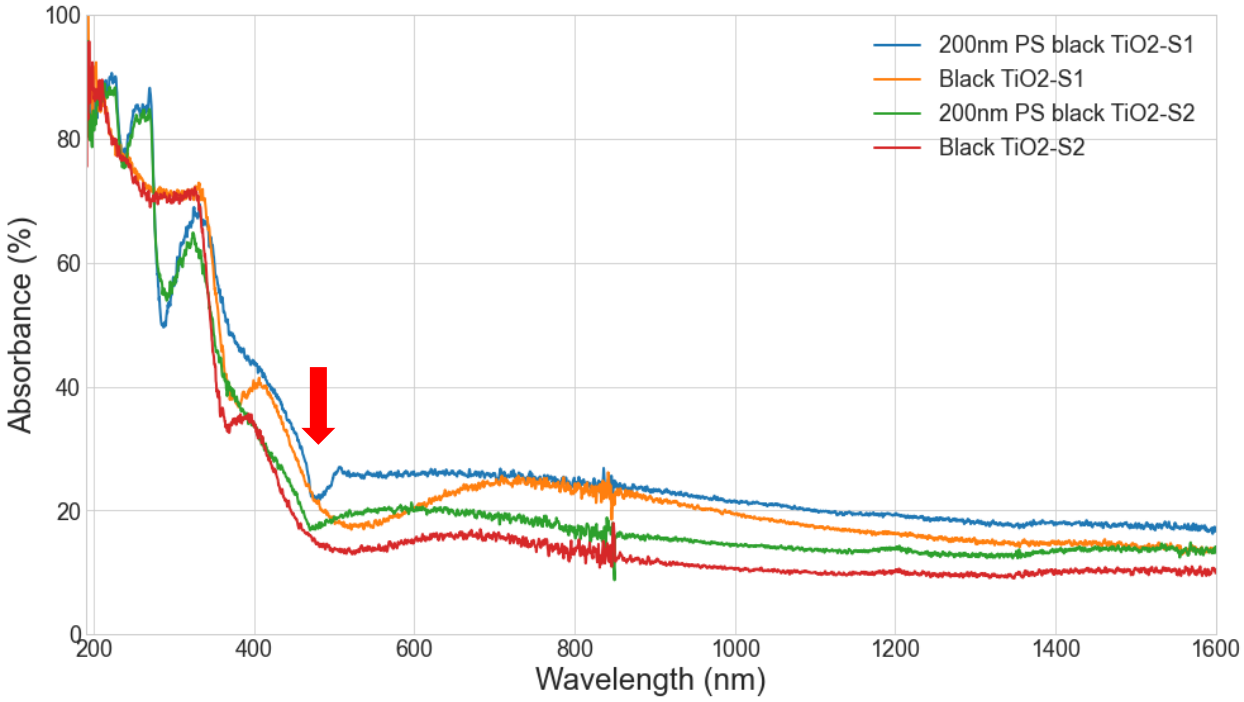

Figure 4.4 Absorbance values for black TiO_2 thin film on quartz wafers before and after deposition of a monolayer of 200nm polystyrene (PS) spheres. The arrow shows the region of increased reflection.

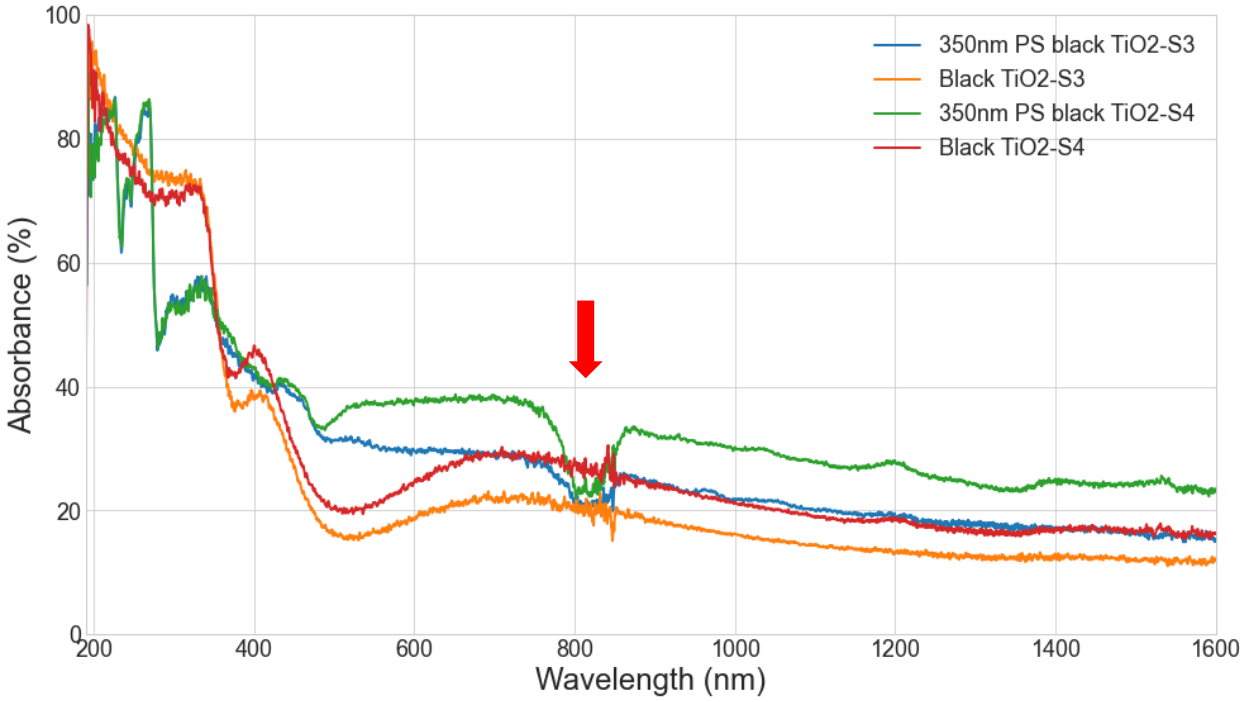

Figure 4.5 Absorbance values for black TiO_2 thin film on quartz wafers before and after deposition of a monolayer of 350nm polystyrene (PS) spheres. The arrow shows the region of increased reflection.

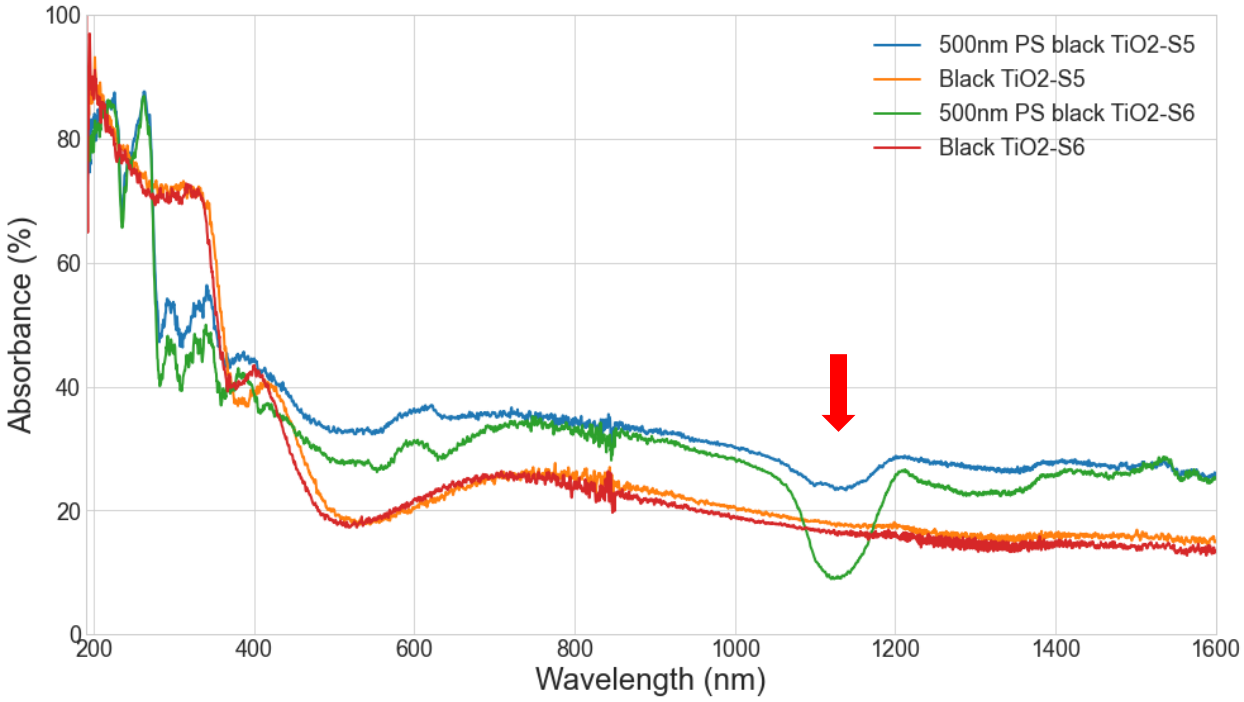

Figure 4.6 Absorbance values for black TiO_2 thin film on quartz wafers before and after deposition of a monolayer of 500nm polystyrene (PS) spheres. The arrow shows the region of increased reflection.

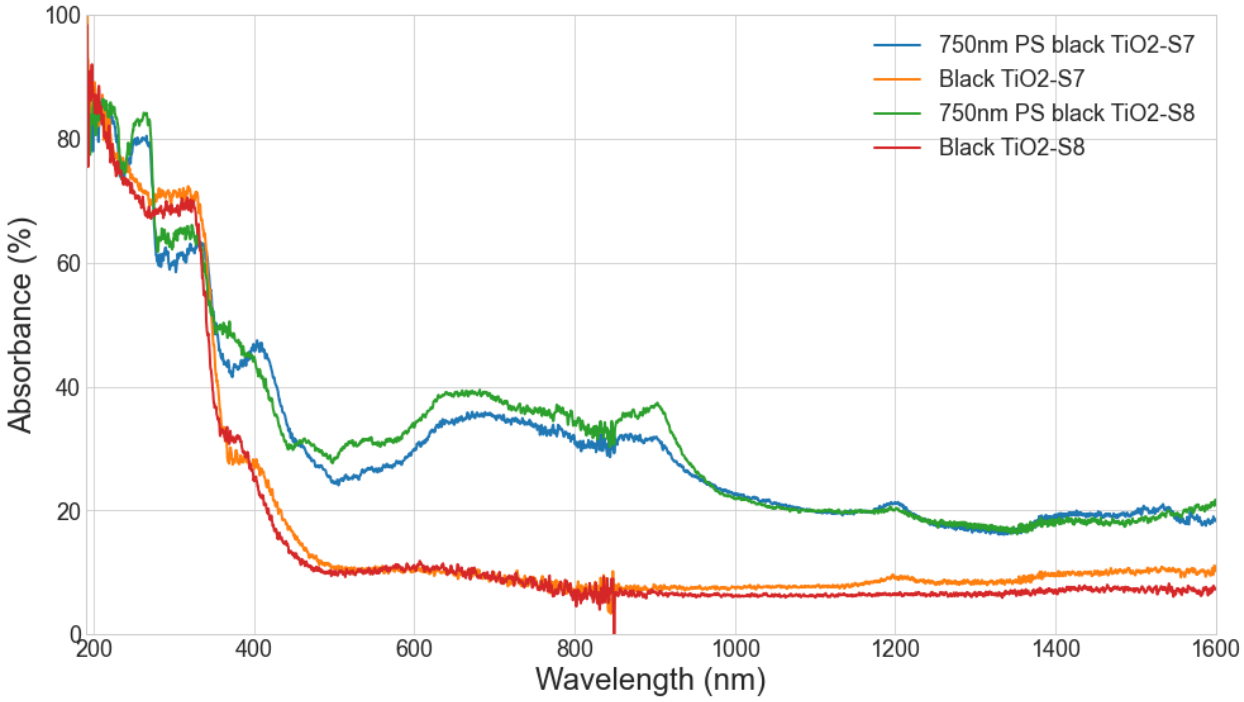

Figure 4.7 Absorbance values for black TiO_2 thin film on quartz wafers before and after deposition of a monolayer of 750nm polystyrene (PS) spheres.

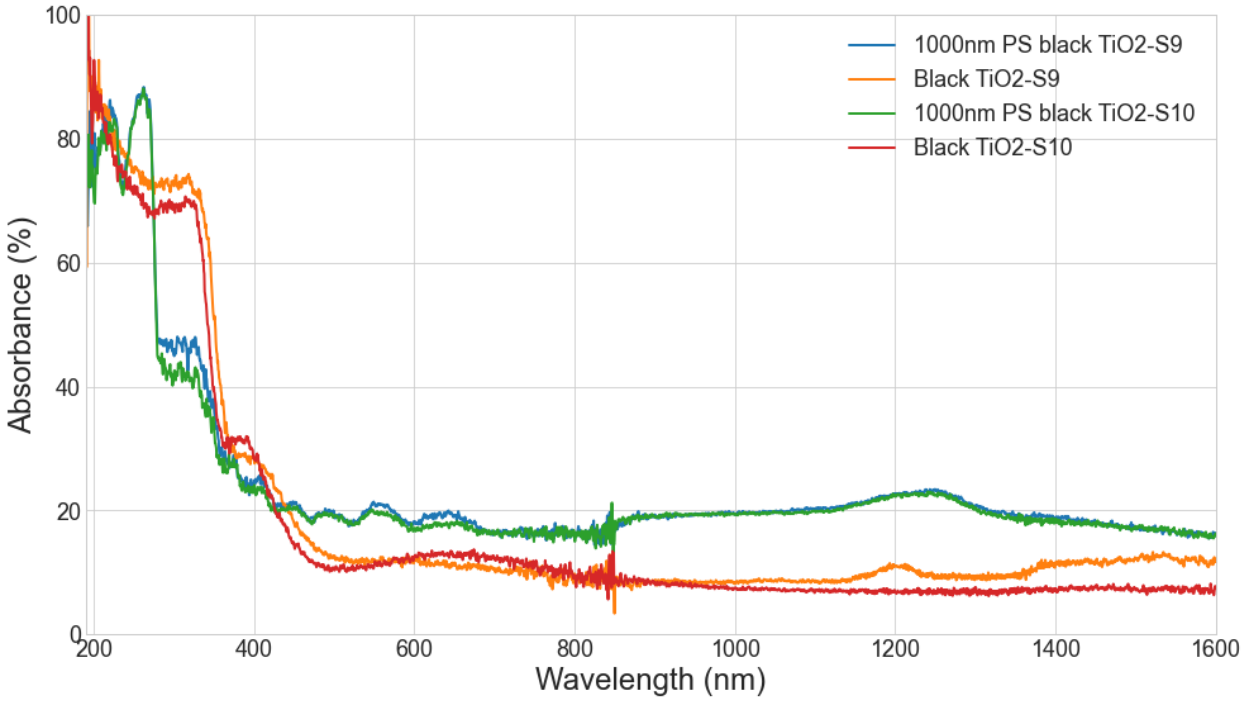

Figure 4.8 Absorbance values for black TiO_2 thin film on quartz wafers before and after deposition of a monolayer of 1000nm polystyrene (PS) spheres.

colloids, with the one on the right has a coating of 350nm polystyrene colloids. Both samples were coated using the slow evaporation method and both suspensions were diluted to 0.005% (w/w%) of colloids in water. Figure 4.9 shows that the size difference of the colloids requires an adjustment to the solution concentration be done to obtain the monolayer of colloids when the diameter is varied. The larger the colloids are, the less dilute of solution will be needed to create a monolayer. The smaller the colloids diameter becomes, the more dilute the solution must be to create the desired uniform monolayer on the surface of the substrate.

The samples viewed using this method, as shown in Figure 4.9, were placed in the ALD to be coated with a ZnO layer. Due to the sphere material being polystyrene, the chamber and door heat of the ALD could not exceed 80°C to maintain the structure of the spheres and keep them from melting. Each cycle of the ZnO process included sequential exposures to diethylzinc (DEZ) and H_2O precursors from room-temperature cylinders. Each DEZ exposure consisted of a precursor pulse (22 ms under 40 sccm N_2 carrier gas flow), a precursor soaking step to maximize the exposure (1 s, 40 sccm N_2 with the pump valve closed), and a purge step to evacuate the chamber of the precursor (15 s, 100 sccm N_2). Each H_2O exposure consisted of a precursor pulse (22 ms, 40 sccm N_2), a soaking step (1 s, 40 sccm N_2 with the pump valve closed), and a purge step (15 s, 100 sccm N_2). This cycle was repeated 200 times.

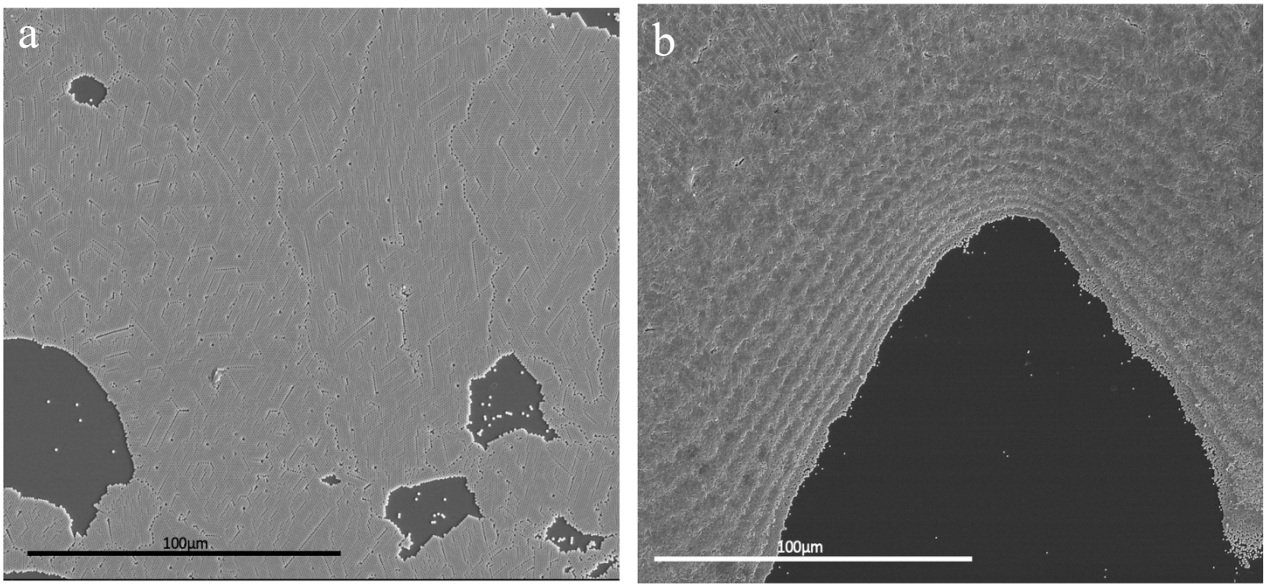

Figure 4.9 (a) sample has a coating of 750nm polystyrene colloids and sample (b) has a coating of 350nm polystyrene colloids. Both solutions contained 0.005% (w/w%) colloidal concentration.

4.4: Discussion

After initial trials with spin coating were unsuccessful due to the extensive and potentially destructive cleaning process that would be required for the substrate surface to be adequately hydrophilic, slow evaporation was implemented. The slow evaporation method allowed for a gentler cleaning process to be used to prepare substrates for deposition. Slow evaporation also gave more consistent results for the monolayer across multiple samples making it the better option even though the process takes more time to complete.

After the deposition process was determined and perfected for a monolayer coating of colloids, deposition on the black TiO_2 coated quartz samples was completed. UV-Vis measurements were taken of each sample before and after colloidal deposition of PS spheres (diameters were 200nm, 350nm, 500nm, 750nm, and 1000nm). An increase in absorption was noted for all samples across all diameters from approximately 360nm to 1600nm. There is an exception to this general increase for the sphere diameters of 200nm, 350nm, and 500nm. For the 200nm PS spheres, the increase in reflection is around 475nm, 350nm PS spheres shows an increase in reflection around 815nm, and 500nm PS spheres shows an increase in reflection around 1115nm. Due to opalescence of the nanospheres, an increase in reflection occurs which causes a decrease in the absorption. At these wavelengths for the 200nm, 350nm, and 500nm spheres, the spheres are not needed as the black TiO_2 has better absorption without them.

References

(1) Ni, H.; Liu, X.; Cheng, Q. A new strategy for air-stable black phosphorus reinforced PVA nanocomposites. *Journal of Materials Chemistry A* **2018**, *6* (16), 7142-7147, 10.1039/C8TA00113H. DOI: 10.1039/C8TA00113H.

(2) Aguirre, C. I.; Reguera, E.; Stein, A. Tunable Colors in Opals and Inverse Opal Photonic Crystals. *Advanced Functional Materials* **2010**, *20* (16), 2565-2578. DOI: https://doi.org/10.1002/adfm.201000143.

(3) Reed, P. J.; Mehrabi, H.; Schichtl, Z. G.; Coridan, R. H. Enhanced Electrochemical Stability of TiO2-Protected, Al-doped ZnO Transparent Conducting Oxide Synthesized by Atomic Layer Deposition. *ACS Applied Materials & Interfaces* **2018**, *10* (50), 43691-43698. DOI: 10.1021/acsami.8b16531.

(4) George, S. M. Atomic Layer Deposition: An Overview. *Chemical Reviews* **2010**, *110* (1), 111-131. DOI: 10.1021/cr900056b.

(5) J M Jasinski; B S Meyerson, a.; Scott, B. A. Mechanistic Studies of Chemical Vapor Deposition. *Annual Review of Physical Chemistry* **1987**, *38* (1), 109-140. DOI: 10.1146/annurev.pc.38.100187.000545.

(6) Park, B.; Na, S. Y.; Bae, I.-G. Uniform two-dimensional crystals of polystyrene nanospheres fabricated by a surfactant-assisted spin-coating method with polyoxyethylene tridecyl ether. *Scientific reports* **2019**, *9* (1), 1-9.

(7) Jiang, P.; McFarland, M. J. Large-Scale Fabrication of Wafer-Size Colloidal Crystals, Macroporous Polymers and Nanocomposites by Spin-Coating. *Journal of the American Chemical Society* **2004**, *126* (42), 13778-13786. DOI: 10.1021/ja0470923.

Chapter 5: Monolithic, Integrated Structures for Light Trapping based on Nanosphere Monolayers

The general need for increasing light absorption in ultra-thin films has been discussed in previous chapters. For THz emission applications, thin films are used to maximize electron transport effects and minimize unintended reabsorption of THz radiation. This generally requires the use of direct band gap semiconductors like GaAs, which have short absorption lengths (α^{-1}). Additionally, there is an interest in using ultra-thin two-dimensional (2D) materials such as MoS_2 and black phosphorous (BP), which have tailorable band gaps depending on the number of layers included.

In the previous chapters, we showed that a monolayer of self-assembled nanospheres could be used to improve light absorption through a combination of light scattering (surface roughening) and optical resonances generated by the regular structure of refractive index contrast. Another strategy that can be used for increasing light trapping is to add a planar dielectric layer over the thin film itself. The addition of this quarter-wave plate can prevent light reflected from internal interfaces from escaping the absorber. The quarter wave plate aids in trapping light above the black phosphorus due to its higher index of refraction. It can also prevent deleterious chemical reactions that can occur between the semiconductor and the environment. For example, BP is susceptible to oxidation in air or in humidity, which would disturb the semiconducting properties of the material.[1] A layer of hexagonal boron nitride with an intentionally chosen thickness can act as both a protection layer from chemical reactions and as a quarter-wave plate.

Related to unwanted chemical transformations in the semiconductor, the nanosphere self-assembly process we showed in Chapter 3 is slow (~48 hours) and carried out in aqueous

solutions that may harm the semiconductor layer under similar oxidative conditions. The placement of the monolayer of nanospheres can also be of critical importance. THz generation is induced by the localized absorption of a laser focused through a microscope objective, rather than large area absorption that drives a photovoltaic in previous studies.[2] The resonances that are intended to trap light are generated by large area crystalline domains, acting as a practically infinite lattice without defects, dislocations, or gaps. Aligning the incident laser beam with the area of highest practical crystallinity is a priority. Further, for some materials the orientation of this perfect crystal can potentially be important. BP has anisotropic optical properties (Figure 5.1[1]), where the polarization vector of the incident illumination determines the absorption. The relative orientation of the lattice of the nanosphere layer can potentially impact the ability to couple the favorable light concentrating resonances into the photoconductive absorber layer. This issue was not an important consideration in GaAs-based THz emitters or in the TiO_2 work described in previous chapters, as those materials have isotropic dielectric properties.

An ideal solution to these complications would be to fabricate these functional layers into a transferrable, orientable structure that can be placed onto the THz device after completion. Fabricating a monolithic light trapping architecture on a transferrable substrate would provide many advantages over the direct fabrication of a self-assembled layer of nanospheres on a semiconductor surface. The deposition of the dielectric layers can be controlled precisely via ALD or other methods such as sputtering or evaporation. The self-assembled nanosphere layer can further act to template more dielectric contrast through infiltration. The transfer of the structure to the THz device allows for the most crystalline region of the nanosphere layer to be placed coincident with the laser beam. The orientation of the nanosphere layer can also be adjusted to maximize absorption in anisotropic materials such as BP. Finally, separating the

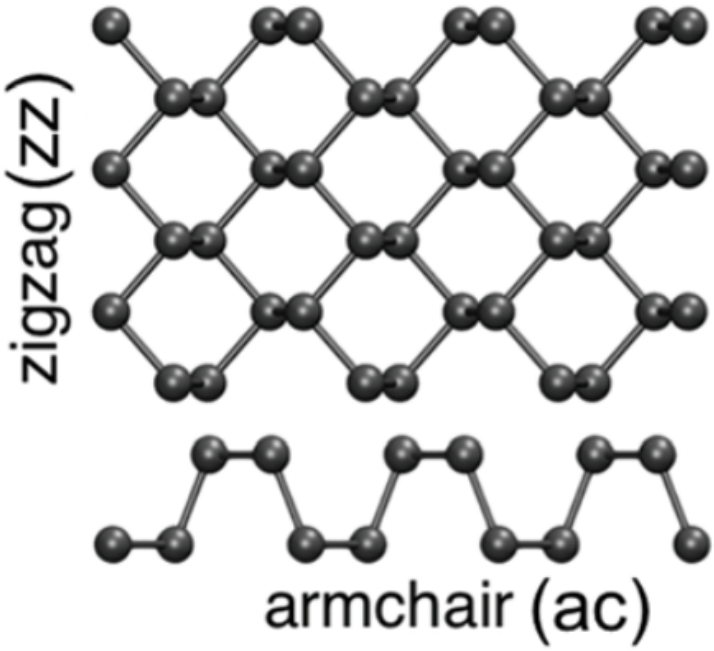

Figure 5.1 View of the zig zag and armchair structures of black phosphorus. (Reprinted with permission from reference 1. Copyright © 2018 Royal Society of Chemistry)

fabrication of the light trapping structure can avoid the potential deleterious effects that those conditions could have on the light absorbing layer. For example, the high temperature and humidity of an ALD reaction, the high surface temperatures generated in thermal or electron-beam evaporation, ion bombardment in a sputtering plasma, or even the aqueous submersion environment for nanosphere self-assembly can impact the performance and properties of the semiconductor or damage the metal antenna structure.

To address the potential advantages of a monolithic integrated light concentration strategy, we translated the previous approach combining finite-element time-domain (FDTD) simulations, chemical materials synthesis via ALD, and the self-assembly of hexagonally close-packed (hcp) monodisperse nanospheres to a transferrable quartz wafer substrate. Given the previous results that showed particular combinations of sphere layers, diameters, and refractive indices could generate an enhanced absorption in thin GaAs layers, we hypothesized building an integrated device with spheres directly in contact with the photoconductive absorber layer on a different substrate would also enable us to consider more flexible design, including a quarter wave plate dielectric layer above and below the spheres, multiple dielectric materials in the integrated device, and the opportunity to invert the dielectric structure based on the nanosphere template. A schematic of this interface is shown in Figure 5.2c and e. As a result of this design, all these free parameters can be tuned to maximize the electric field concentration and absorption directly at the interface of the spheres and the photoconductive absorber layer.

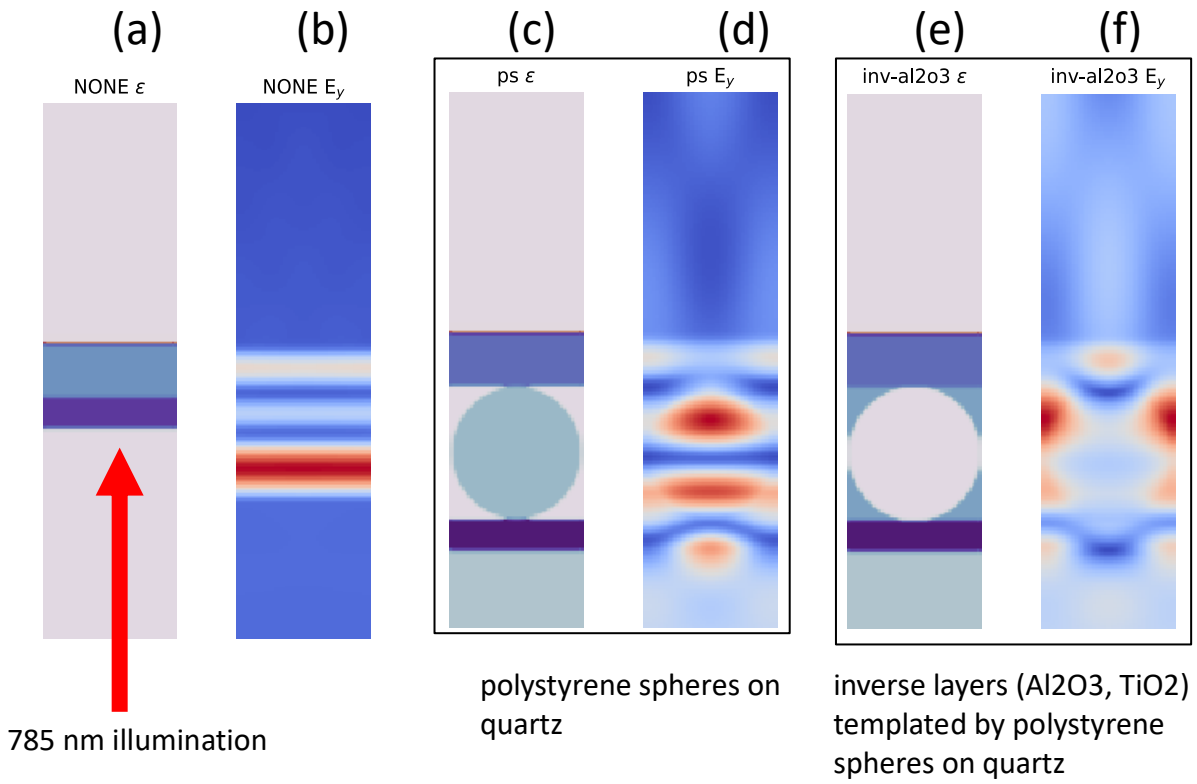

Figure 5.2 Examples of (a, c, e) of the monolith geometry and the corresponding (b, d, f) FDTD generated steady-state electric fields for 785nm illumination in a planar (a, b) TiO_2/hBN layers, (c, d) TiO_2/PS nanosphere/hBN, and (e, f) TiO_2/inverse structure Al_2O_3 templated by spheres/hBN.

5.1: FDTD simulations of a monolithic, light concentrating chip

The large parameter space for designing this integrated monolith makes direct fabrication of structures with notable light concentrating properties impossible. Numerical simulation is required to help identify the optimal combination of all the design parameters to maximize the desired light concentration effects. We used FDTD simulations to explore the collective relationship of all these parameters to identify structures for experimental fabrication. It is also important to note a few practical points about the choices for the monolith structure. Quartz may not be an ideal substrate for THz generation. The large quartz wafer pieces we work with (smallest ~few mm^2) are large compared to the entire THz antenna device (gap = 10um). The quartz wafer could potentially alter the THz emission by affecting the dielectric environment around the metal antennas. This has not been shown to be a deleterious issue but is a concern that needs to be considered in THz simulations. We are using quartz in these simulations because it is a practical substrate that allows us to both simulate and fabricate the monolith to test the light trapping part. Once we identify the appropriate strategy in ways that we can confirm experimentally, the miniaturization of that structure would be an important goal for future work.

The FDTD simulations we performed used an open-source package called Meep, which implements the FDTD simulation and the geometric primitives (spheres, slabs, blocks, etc.) that describe the refractive index and optical extinction of the nanostructure.[3] The basic absorber structure for our simulations is to identify the appropriate structure of a nanosphere-templated coating on a quartz wafer that will maximize absorption in the thin GaAs layer when the quartz wafer is placed on the absorber structure. The nanosphere-templated coating is in direct contact with the GaAs layer, inducing near field optical effects. The alternative orientation (with the spheres in the optical far-field) would induce unwanted scattering of the focused laser

illumination. To again represent the connection between simulations and experiments, we chose to simulate the nanosphere diameters that are readily available in the lab rather than a broad search through diameters. The mismatched scales of the GaAs layer thickness (40nm) and the relatively large diameter of the spheres (up to 1000nm) required for a small voxel size (dx = 10nm) and the minimum simulation volume necessary to represent the structure. We used a box where the lateral (x, y) dimensions were defined by the unit sell of the nanosphere hcp lattice (Figure 5.3) and extended by periodic boundary conditions. The top and bottom (z dimensions) of the box used the perfectly matched layer boundary that is used in FDTD simulations to represent propagation away from the cell.[4] The illumination source was a pulsed plane wave with a defined central wavelength, λ= 785 nm, and the Fourier-transformed electric fields were save at this central wavelength. The width of the pulse, df, was chosen to be 10% of the central frequency, $f = c / \lambda$, to ensure numerical stability of the simulation. This procedure isolates the steady-state absorption profile for the central wavelength and identifies the structures that generates notable increases in absorption in the 40nm GaAs layer through a combination of optical resonance and scattering.

A schematic of the monolith structure is shown in Figure 5.2. The specific parameters we varied to optimize the structure were:

- the thickness of a planar dielectric layer between the spheres and quartz (n = 1.46) – this layer was chosen to be TiO_2 for its high index of refraction (n = 2.52 at 785 nm) and our ability to make it via ALD, varied between 0 and 400 nm thick,

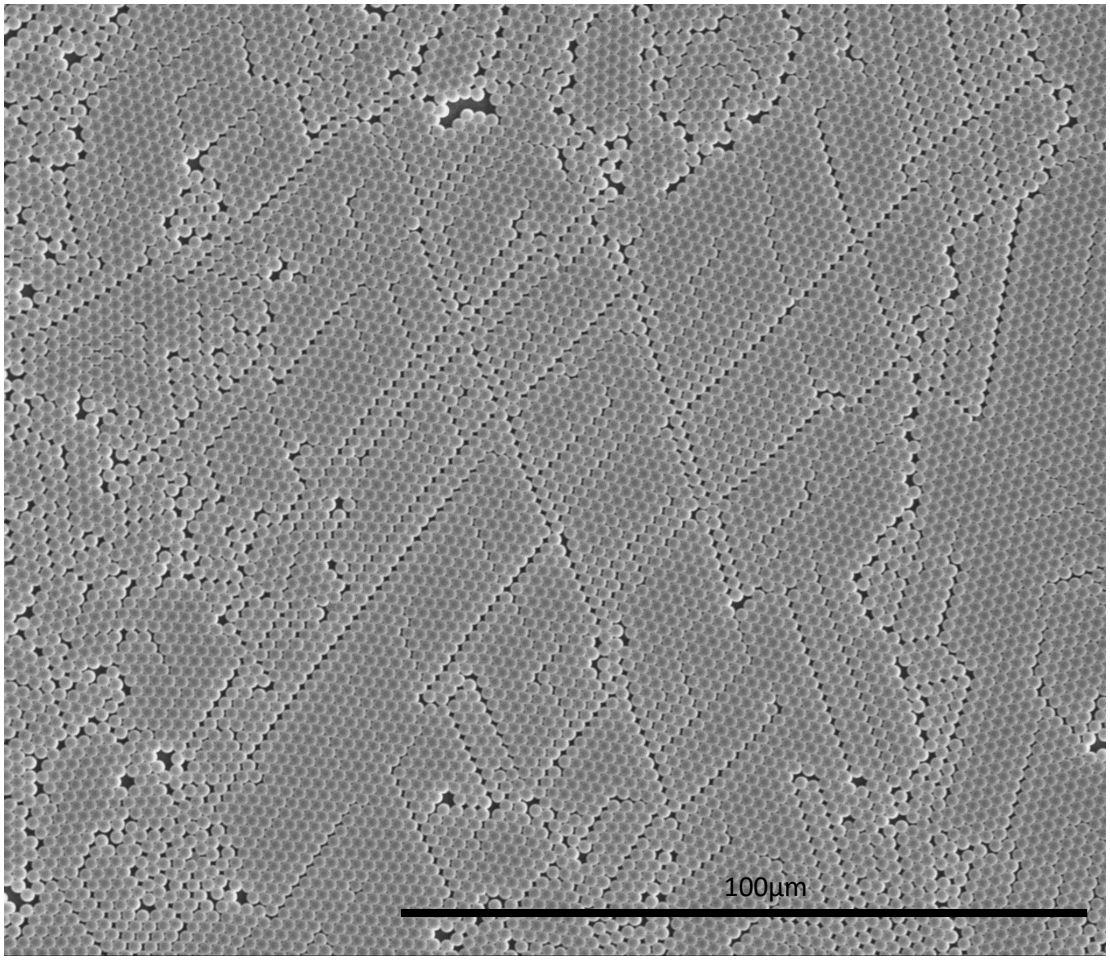

Figure 5.3 SEM image of hexagonally close-packed 750nm PS spheres coated with ZnO.

- the thickness of the quarter waveplate making direct contact with the GaAs layer on the THz photoconductive absorber substrate – this layer was chosen to be hexagonal boron nitride (hBN; n = 2.10 at 785nm) to match what is already used in these devices, varied between 0 and 400 nm thick,
- and the nanosphere monolayer, chosen from the diameters of spheres available in the lab (200nm, 350nm, 500nm, 750nm, 1000nm) – the direct structure was chosen to be polystyrene (n = 1.58), while inverse structures were modeled as nanosphere-templated airholes embedded in a SiO_2 (n = 1.46), Al_2O_3 (n = 1.76), or TiO_2 layer. All four constructions can be prepared in the lab.

The FDTD simulation software accepts the structure as a series of geometric primitives (spheres, blocks, etc.) each with the dielectric properties of that material (function of wavelength) then discretizes the dielectric structure onto a 3-dimensional grid. The absorption in the material can be computed from the time-averaged E(x, y, z) that is generated by the FDTD simulation. Absorption in a voxel of a material with dielectric contrast $\varepsilon = \varepsilon_R + i\,\varepsilon_I$ is equal to

(Equation 3) $$absorption\ (x,y,z) = \frac{\varepsilon_i}{2}|E(x,y,z)|^2 dV$$

Where dV is the volume of the voxel.[4] The total absorption in a layer/volume is the integral over the entire volume of interest, which allows us to separate the ultra-thin GaAs layer from the Si substrate in the absorption calculations. The dielectric contrast is related to the refractive index (n) and the extinction coefficient (k) in both the ε_R and ε_i as follows[5]:

(Equation 4) $$\varepsilon_R = n^2 - k^2$$

(Equation 5) $$\varepsilon_i = 2nk$$

An example of the steady state electric field near a monolithic layered structure (without the nanosphere monolayer) is shown in Figure 5.2b. The polarization of the incident light was

oriented in a direction that is perpendicular to the surface normal. Figure 5.2a shows a two-dimensional slice through the layered structure of a quartz wafer coated with a layer of TiO_2 and placed onto a GaAs-coated Si substrate with a hexagonal boron nitride (hBN) quarter wave plate between them. The amplitude of the steady state electric field, $|E(x, y, z)|^2$, is shown in Figure 5.2b. A slice through of a monolithic structure composed of a 750nm polystyrene (PS) microsphere layer, 200nm of TiO_2 on quartz, and a 400nm layer of hBN on a 40nm GaAs/Si photoconductive absorber layer is shown in Figure 5.2c. To somewhat simplify the discussion, we refer to this structure as 200nm TiO_2/750nm PS/400nm hBN. The steady magnitude of electric field, $|E(x, y, z)|^2$, for the same structure is shown in Figure 5.2d. The three-dimensional sphere layer traps light near the surface and scatters it into off-normal directions, either localizing the electromagnetic energy in resonances or by simply increasing the path length of light through the 40nm GaAs layer. Both effects contribute to the total absorption of light in the GaAs as calculated from the total integral of Equation 2 in the volume of the GaAs. As these simulations are linear in the overall intensity of the incident pulse, we can use the simple null case of an uncoated quartz wafer in direct contact with the GaAs layer, without TiO_2 or hBN, as the reference for absorption in all other monolithic structures. To ensure compatible comparisons, we normalized the absorption to the projected geometric area of the unit cell used in the simulation.

The first structure we simulated was the direct monolith, composed of a monolayer of polystyrene nanospheres (n = 1.58) on an ordinary TiO_2-coated quartz substrate placed on an hBN layer over GaAs. The role of the TiO_2 is to trap light scattered away from the interface by the sphere layer. We performed the simulations as a function of the nanosphere diameter (d= 200nm, 350nm, 500nm, 750nm, or without spheres), the thickness of the TiO_2 layer (T_{TiO2} = 0-

400 nm, 40nm steps), and the thickness of the hBN layer (T_{hBN} = 0-400 nm, 40nm steps) to identify particularly useful combinations of materials for maximizing light absorption at a central wavelength of excitation (785nm) used for the simulation of the THz emitter.

The basic one-dimensional structure, without spheres, showed a roughly 3.0x enhancement in absorption compared to the null case (no spheres, T_{TiO2} = 0nm, T_{hBN} = 0nm) centered on an hBN layer that was roughly 200nm thick. This enhancement was relatively independent of the thickness of the TiO_2 layer. The addition of a 200nm (Figure 5.4b) or 350nm (Figure 5.4c) nanosphere monolayer showed similar behavior to the structure without spheres, likely due to the small diameter of the spheres. There was some dependence on T_{TiO2} observed within the band of peak absorbance near T_{hBN} = 200nm. The maximum absorbance is roughly 2.3x for a 120nm TiO_2/200nm hBN monolith and 2.0x for 160nm TiO_2/350nm PS/240nm hBN monolith. We observed stronger absorption in the GaAs layer for several monolith structures based on a direct monolayer of 500nm PS spheres (Figure 5.4d). Structures with maximal absorption include the 80 nm TiO_2/500 nm PS/200 nm hBN (8.0x enhancement) and 240nm TiO_2/500 nm PS/240 nm hBN (9.0x enhancement). The maxima in the absorption profiles are relatively broad and periodic along the T_{hBN} = 240 nm band, suggesting that the effect would be relatively robust versus some degree in polydispersity in the PS nanosphere layer. For a 750 nm PS layer, the resonances are muted compared to the 500 nm PS. For example, the maximum absorption is roughly 4.0x for the 120 nm TiO2/750 nm PS/280 nm hBN and the 280 nm TiO2/750 nm PS/280 nm hBN monoliths.

We also studied the fabrication of inverse layers (air holes in solid films) templated by a monolayer of PS nanospheres. The choice of materials for the direct nanosphere layer is limited to PS or SiO_2 if a reasonable level of monodispersity is desired. However, both materials have

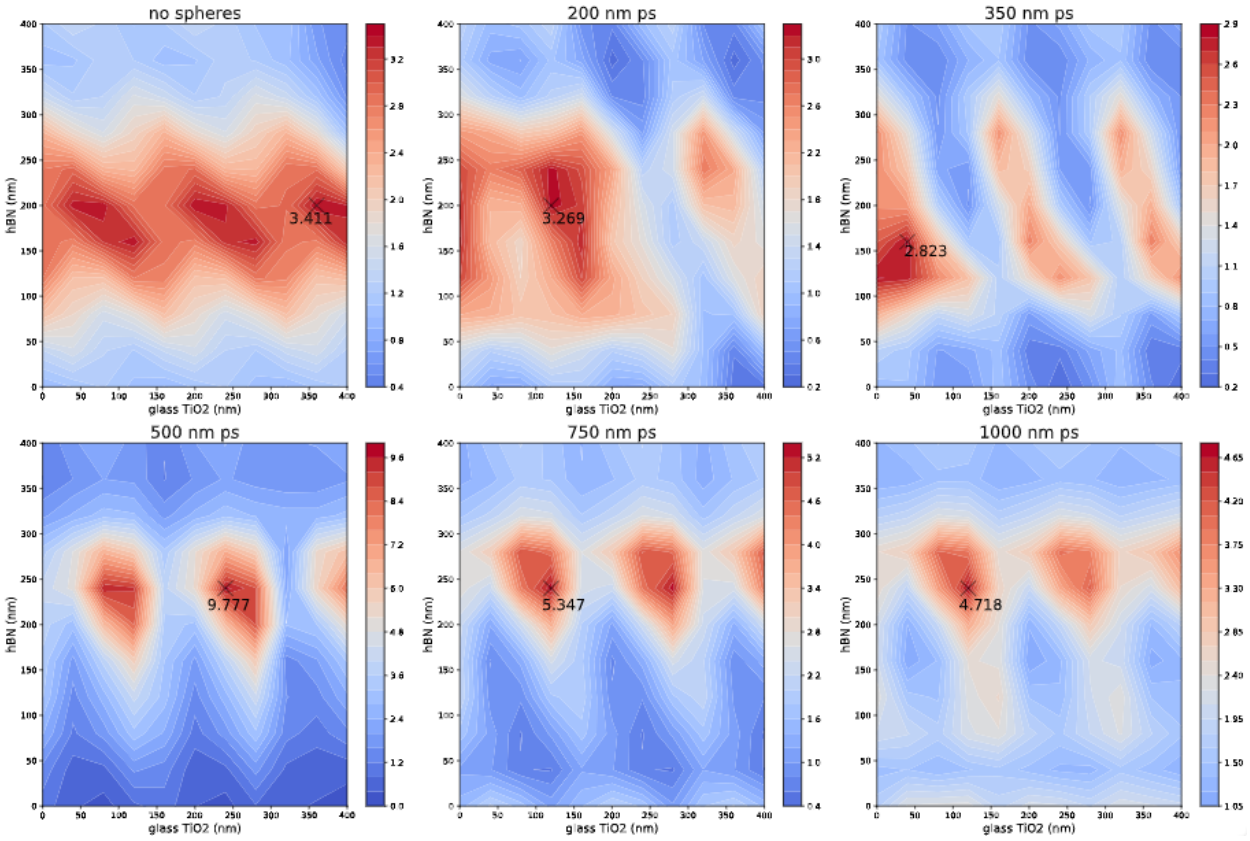

Figure 5.4 Simulation data of the monolith structure with no spheres, 200nm, 350nm, 500nm, 750nm, and 1000nm PS spheres on a quartz TiO_2 layer (0-400nm, 40nm increments, x-axis) with an hBN top layer (0-400nm, 40nm increments, y-axis). This data shows the enhancements in the absorption for the various parameters.

relatively low refractive indices, limiting the magnitude of the scattering to the dielectric contrast between the air and spheres. The promise of an inverse structure is twofold: (a) the inverse opal has a photonic band gap, and an inverse monolayer will have unique optical properties compared to the direct monolayer, and (b) the inverse structure can be synthesized from virtually any metal oxide by infiltration methods (sol gel or electrodeposition, for example) or by ALD. As a result, materials with higher refractive indices can be used to generate higher dielectric contrast and increased scattering with the monodispersity of the holes templated by the nanosphere layer.

Here we simulated inverse monoliths using Al_2O_3 (n = 1.9; Figure 5.5) and ordinary TiO_2 (n = 2.2; Figure 4.6), as we can fabricate these structures easily with ALD. The inverse Al_2O_3 monolith showed similar qualitative behavior to the small feature, direct PS monoliths for the one-dimensional, 200 nm air hole, and 350 nm air hole monoliths. The larger-sphere inverse Al_2O_3 monolith structure exhibited similar oscillatory dependence on the TiO_2 thickness along the T_{hBN} = 240 nm band, peaking at a 10.0x enhancement for the 40 nm TiO_2/500 nm inv-Al2O3/280 nm hBN monolith and 12.0x for the 120 nm TiO_2/750 nm inv-Al_2O_3/240 nm hBN monolith. These peaks showed a broader dependence on T_{hBN} and T_{TiO2} for the 750 nm inverse-Al_2O_3 monoliths than for the 500 nm inverse-Al_2O_3 monoliths. An inverse structure prepared from TiO_2 increased the dielectric contrast between material and the air holes, resulting in significantly stronger absorption peaks in both 500 nm inverse-TiO_2 and 750 nm inverse-TiO_2 monolith structures. Of all the simulations described here, the 40 nm TiO_2/500 nm inv-TiO_2/400 nm hBN monolith showed the largest absorption enhancement (20.5x versus the null case), though with a particularly sharp dependence on the structural parameters. The 750 nm inverse-TiO_2 monolith showed several more broad resonances with high (13.0x for 240 nm TiO_2/750 nm inv-TiO_2/120 nm hBN) absorption enhancements in the GaAs layer.

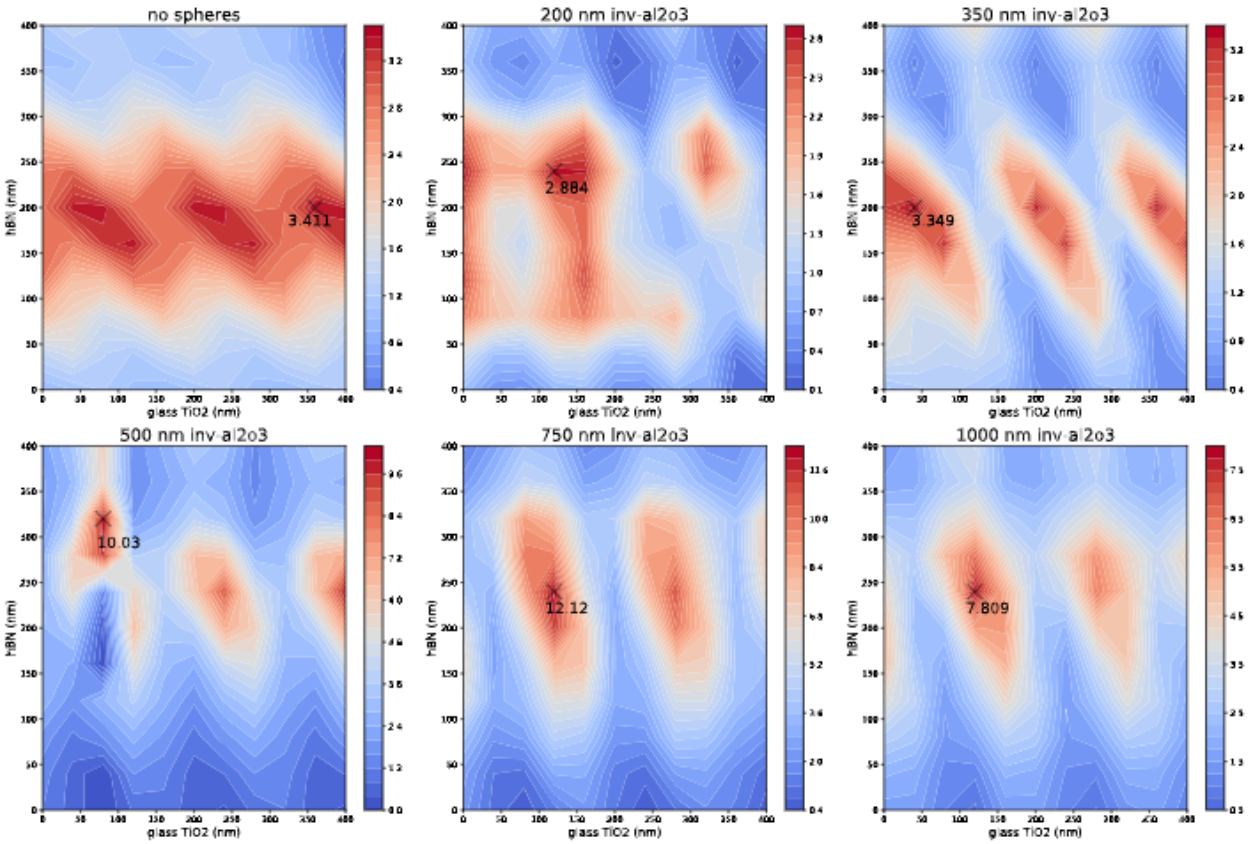

Figure 5.5 Simulation data of the monolith structure for the Al_2O_3 inverse-sphere layer using no spheres, 200nm, 350nm, 500nm, 750nm, and 1000nm PS spheres as a template on a quartz TiO_2 layer (0-400nm, 40nm increments, x-axis) with an hBN top layer (0-400nm, 40nm increments, y-axis). This data shows the enhancements in the absorption for the various parameters.

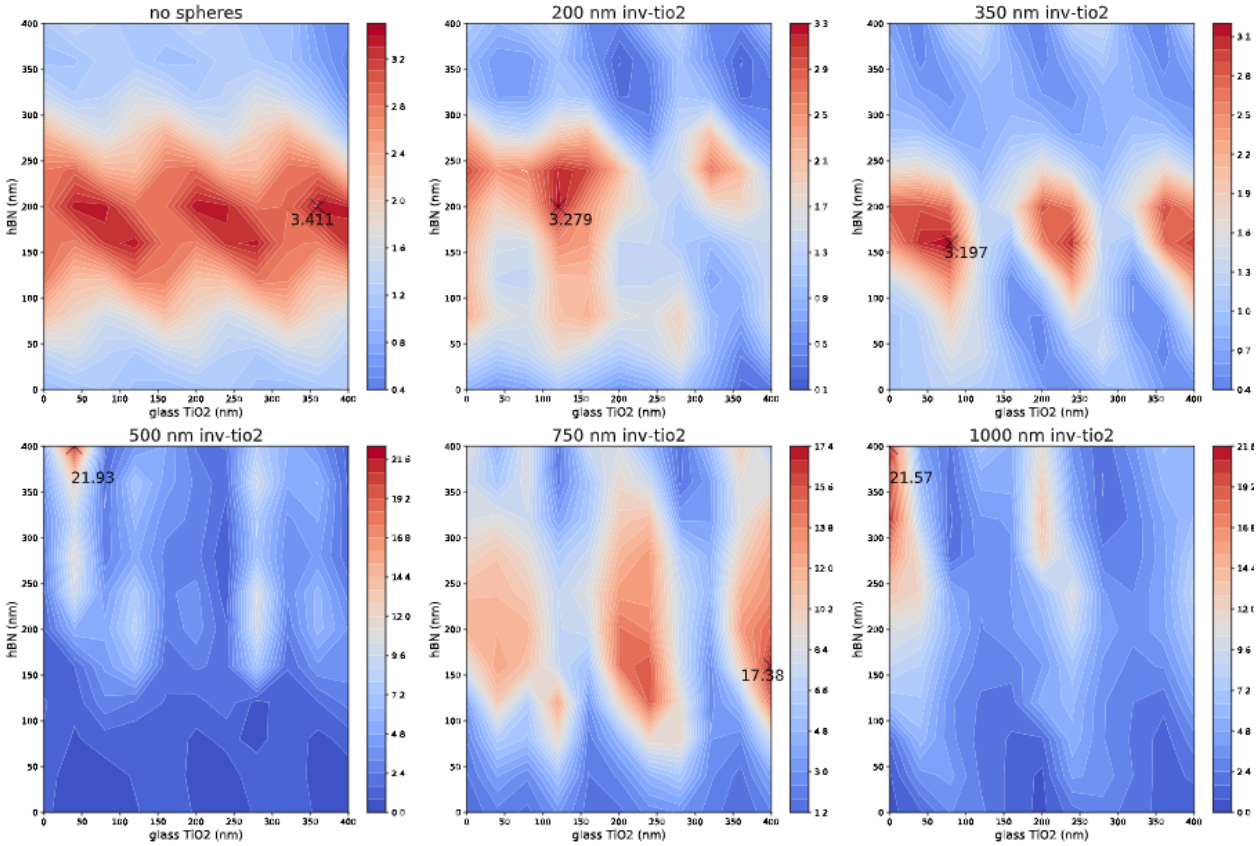

Figure 5.6 Simulation data of the monolith structure for the TiO_2 inverse-sphere layer using no spheres, 200nm, 350nm, 500nm, 750nm, and 1000nm PS spheres as a template on a quartz TiO_2 layer (0-400nm, 40nm increments, x-axis) with an hBN top layer (0-400nm, 40nm increments, y-axis). This data shows the enhancements in the absorption for the various parameters.

The results of these simulations suggest additional degrees of freedom to explore. The removal of the PS template could be particularly difficult with the inclusion of the infiltration layer. The template will potentially become encapsulated by the infiltration layer. While this somewhat reduces the achievable dielectric contrast (with the air holes replaced by PS), encapsulation may be a useful approach to mechanical stability of the structure. Avoiding the difficulty of removing the template could lead to a fully integrated monolith, including a layer to provide the same functional effect as the hBN layer, though with the added ease of continued ALD growth.

5.2: Experimental Synthesis

Synthesizing the monolith structure is done via a multistep process which uses ALD and slow evaporation methods previously mentioned in Chapter 4. While these methods are used to develop the monolith structure, there are many differences to note. The deposition process of the spheres is not the same when coating different surfaces. Previously the spheres have been deposited onto quartz, glass, and quartz coated with black TiO_2. Quartz without any coatings requires the surface to be cleaned through sonication (acetone, methanol, isopropanol, and DI water for 15 minutes each) but also requires a longer time in the UV-ozone cleaner (1 hour) to ensure the surface is hydrophilic enough for the spheres to adhere. Glass substrates do not have the best deposition due to the nature of the surface. Unless the glass has a more optically flat surface, the spheres typically rest in the valleys of the surface and not the entirety. This causes large gaps to occur when the film should be a more uniform coating covering large areas. Quartz with ALD coatings (like black TiO_2) had better success with deposition of the spheres.

The use of the ALD to develop the structure also has some differences. While in Chapter 4 the ALD was used to create the black TiO_2 layer with a process that better reflected chemical vapor deposition, the ALD will be used for its original purpose when creating the monolith structure. Some of the coatings that can be deposited in our lab include TiO_2, ZnO, and Al_2O_3. These coatings do not need to be created at the high temperature that the black TiO_2 layer was deposited at (300°C).

For the deposition of a TiO_2 film, the precursor TDMAT and H_2O are used. The reactor chamber is set to 150°C and the TDMAT precursor cylinder is heated to 80°C during the process. The H_2O was set at room temperature. Each cycle consists of pulses of the TDMAT (100ms, purge of 15s) and H_2O (15ms, purge of 25s). This process is similar for the deposition of the thin films Al_2O_3 and ZnO. The difference is the use of the appropriate precursors trimethylaluminum and diethylzinc respectively. When coating the regions around the spheres, this will require a longer period for the precursors and H_2O to soak into the structure. By increasing the time between pulses and the flow of nitrogen through the reactor chamber, this allows for the precursors to settle in the small openings between the spheres.

5.3: Characterization

Characterization of the monolith structures can be done using the SEM and UV-Vis spectrometer. The SEM allows for us to view the monolith structure. The cross-sectional view of the structure is obtained by breaking the entire structure to get a view of each component of the structure. When depositing the inverse structure on the monolith, using the SEM will aid in determining the appropriate number of cycles needed in the ALD. Knowing the adequate number

of cycles to complete the inverse structure is important so that there is not an added layer above the completed inverse structure occurs which would add extra layers in the monolith structure.

The UV-Vis will aid in the determination of the absorption by obtaining the reflectance and transmittance measurements. The measurements are inputted into Equation 1 to determine the absorption of each sample measurement. These measurements can be taken in between each added component of the monolith structure to determine the increase in absorption that occurs with each step. Ultimately, the UV-Vis measurements will aid in determining the potential increase in absorption that may occur when the monolith structure is implemented onto the THz device.

References

(1) Gaberle, J.; Shluger, A. L. Structure and properties of intrinsic and extrinsic defects in black phosphorus. *Nanoscale* **2018**, *10* (41), 19536-19546.

(2) Grandidier, J.; Callahan, D. M.; Munday, J. N.; Atwater, H. A. Light Absorption Enhancement in Thin-Film Solar Cells Using Whispering Gallery Modes in Dielectric Nanospheres. *Advanced Materials* **2011**, *23* (10), 1272-1276, https://doi.org/10.1002/adma.201004393. DOI: https://doi.org/10.1002/adma.201004393 (acccessed 2021/02/20).

(3) Oskooi, A. F.; Roundy, D.; Ibanescu, M.; Bermel, P.; Joannopoulos, J. D.; Johnson, S. G. MEEP: A flexible free-software package for electromagnetic simulations by the FDTD method. *Computer Physics Communications* **2010**, *181* (3), 687-702.

(4) Taflove, A.; Hagness, S. C. *Computationai Electrodynamics*; Artech House, 2005.

(5) Wooten, F. *Optical properties of solids*; Academic press, 2013.

Chapter 6: Conclusion

Development of the deposition of colloids was initially done through multiple trials with different methods. After initial trials with spin coating were unsuccessful due to the extensive and potentially destructive cleaning process that would be required for the substrate surface to be adequately hydrophilic, slow evaporation was implemented. The slow evaporation method allowed for a gentler cleaning process to be used to prepare substrates for deposition. Slow evaporation also gave more consistent results for the monolayer across multiple samples making it the better option even though the process takes more time to complete.

After the deposition process was determined and perfected for a monolayer coating of colloids, deposition on the black TiO_2 coated quartz samples was completed. UV-Vis measurements were taken of each sample before and after colloidal deposition of PS spheres (diameters were 200nm, 350nm, 500nm, 750nm, and 1000nm). An increase in absorption was noted for all samples across all diameters from approximately 360nm to 1600nm. There is an exception to this general increase for the sphere diameters of 200nm, 350nm, and 500nm. For the 200nm PS spheres, the increase in reflection is around 475nm, 350nm PS spheres shows an increase in reflection around 815nm, and 500nm PS spheres shows an increase in reflection around 1115nm. Due to opalescence of the nanospheres, an increase in reflection occurs which causes a decrease in the absorption. At these wavelengths for the 200nm, 350nm, and 500nm spheres, the spheres are not needed as the black TiO_2 has better absorption without them.

The FDTD simulation results for the monolith structure show large potential absorptions that may be possible. While the results from the simulation suggest additional degrees of freedom that need to be explored in the future, the simulations showed multiple promising parameters to verify experimentally. Removal of the PS templates may not be obtainable and

require the PS template be included with the infiltration layer. This will somewhat reduce the previously achievable dielectric contrast (with the air holes replaced by PS), but encapsulation of the PS template may aid in the mechanical stability of the inverse structure. Avoiding the difficulty of removing the template could lead to a fully integrated monolith, including a layer to provide the same functional effect as the hBN layer, though with the added ease of continued ALD growth.

Potential future work could include using different materials with higher refractive indices could further increase the potential absorption. Using the readily available colloids, an inverse template could be made to then filled with the desired material. This could be accomplished using processes like ALD or solgel to create the inverse template and subsequently refill the colloidal openings. The simulations and sample construction could also potentially be done for other applications such as solar cells to optimize the absorption of light within the cells.